Heparin-Azithromycin Microparticles Show Anti-Inflammatory Effects and Inhibit SARS-CoV-2 and Bacterial Pathogens Associated to Lung Infections

Brayan J. Anaya[1], Davide D'Angelo[2], Ruggero Bettini[2], Gracia Molina[1], Amadeo Sanz-Perez[3], María Auxiliadora Dea-Ayuela[4], Carolina Galiana[4], Carmina Rodríguez[5], Diego F. Tirado[6], Aikaterini Lalatsa[7], Elena González-Burgos[3*], D.R. Serrano [1,8*]

[1] Pharmaceutics and Food Technology Department, Faculty of Pharmacy, Universidad Complutense de Madrid, Plaza Ramón y Cajal s/n, 28040 Madrid, Spain.

[2] Food and Drug Department, University of Parma, Parco Area delle Scienze 27a, 43124 Parma, Italy.

[3] Department of Pharmacology, Pharmacognosy and Botany, Faculty of Pharmacy, Universidad Complutense de Madrid (UCM), 28040 Madrid, Spain.

[4] Department of Pharmacy, Universidad Cardenal Herrera-CEU, CEU Universitites, Valencia, Spain.

[5] Department of Microbiology and Parasitology, Faculty of Pharmacy, Universidad Complutense de Madrid (UCM), 28040 Madrid, Spain.

[6] Dirección Académica, Universidad Nacional de Colombia, Sede de La Paz, La Paz 202017, Colombia.

[7] CRUK Formulation Unit, School of Pharmacy and Biomedical Sciences, University of Strathclyde, John Arbuthnot Building, Robertson Wing, 161 Cathedral St, Glasgow G4 0RE, UK

[8] Instituto Universitario de Farmacia Industrial, Faculty of Pharmacy, Universidad Complutense de Madrid, 28040, Madrid, Spain.

* Corresponding authors:

Dolores R Serrano – drserran@ucm.es

Elena González-Burgos – elenagon@ucm.es

33 **Graphical abstract**

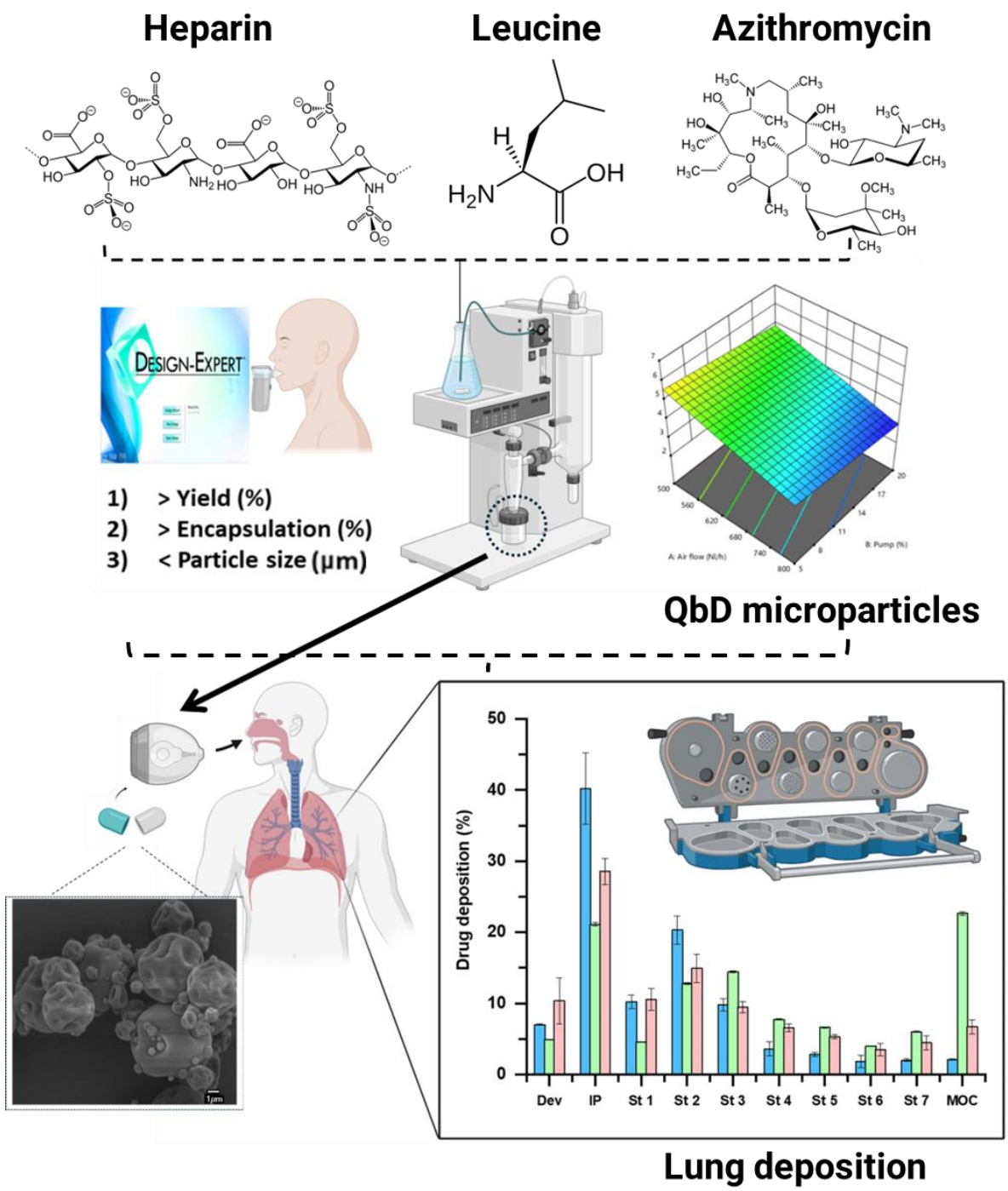

34

35

36

37

Abstract

Pulmonary infections are a leading cause of morbidity and mortality worldwide, a situation exacerbated by the COVID-19. Azithromycin (AZM) is used orally to treat pulmonary infections due to its ability to accumulate in lung tissues and immune cells after oral administration. Sulfated polysaccharides, such as heparin, are known to inhibit SARS-CoV-2 entry. This study presents a novel approach focused on developing a dry powder inhaler of AZM-loaded microparticles composed of either heparin or its derivatives. The microparticle formulations exhibited potent antiviral activity against SARS-CoV-2 ($IC50 \leq 95$ nM) while retaining superior antibacterial efficacy against *Streptococcus pneumoniae* and *Pseudomonas aeruginosa* compared to free AZM (MIC $\leq$ 15 μg/mL). Importantly, at bactericidal concentrations, no cytotoxic effects were observed on mammalian cells, including Calu-3 cells and red blood cells. The formulations demonstrated effective alveolar aerodynamic deposition (MMAD ranging from 1 μm to 3 μm) with a Fine Particle Fraction below 5 μm close to 50 %. Adopting a conservative estimate of 20 mL for the pulmonary epithelial lining fluid volume in healthy adults, efficacious local concentrations of sulfated polysaccharides and AZM would be delivered to the lung using this multifaceted strategy which holds promise for the treatment of bacterial pulmonary infections associated with COVID-19.

Keywords: Heparin, enoxaparin, dry powder inhaler, lung delivery, pulmonary infectious diseases, SARS-CoV-2.

1. Introduction

Lung diseases are the fourth major morbidity and mortality cause in our current society, with cancer and chronic obstructive pulmonary disease (COPD) remaining major challenges. Lung infections are on the rise since the SARS-CoV-2 virus pandemic (COVID-19) started in October 2019 (Franco-Palacios, et al. 2023). Lung diseases caused by various pathogens including bacteria, viruses, and fungi exhibit different trends during COVID-19 (Shi, et al. 2024). COVID-19 can lead to acute respiratory distress syndrome, which can result in pulmonary fibrosis, which can necessitate a lung transplant (Cerier, et al. 2023; Zhu, et al. 2020). In lung cancer patients, COVID-19 increases the mortality rate and severe adverse effects (Calabrò, et al. 2021). Similarly, COVID-19 pneumonia causes various pulmonary complications and increases the mortality risk for patients with chronic lung disease by up to 26 % compared to those without pre-existing lung conditions (Kilic, et al. 2022; Özbek, et al. 2023). Current treatments for COVID-19 remain suboptimal. In the year 2022, COVID-19 still caused 244,986 deaths, with a mortality rate of 61.3 per 100,000 (Ahmad, et al. 2023; Kilic, et al. 2022). Therefore, further research is required to develop targeted approaches beyond oral and parenteral reduced efficacy systemic treatments, which result in a very low drug concentration in the lung parenchyma.

Lung delivery of drugs facilitates the treatment of respiratory bacterial infections and viral diseases, such as COVID-19 (Arauzo, et al. 2021a; Wang, et al. 2023b). Compared to systemic therapies, lung targeting allows for higher drug concentrations in the tissue of interest, reducing systemic exposure and adverse effects (Alipour, et al. 2023; D'Angelo, et al. 2023; de Pablo, et al. 2023; Pradhan, et al. 2022; Tan, et al. 2022). Synergistic effects can be achieved by co-delivering antimicrobials, antivirals, and immunomodulatory drugs within inhalable particles (Celi, et al. 2023b; de Pablo, et al. 2017; Galrinho, et al. 2024).

Sulfated polysaccharides, such as heparin and its derivatives, have gathered significant interest due to their unique properties against COVID-19 (Eilts, et al. 2023; Shi, et al. 2021; Song, et al. 2024b; Wang, et al. 2022). Clinically, two types of heparins (sulfated polysaccharides) are used; (i) unfractionated heparin (UFH) (3 kDa - 30 kDa) and (ii) low molecular weight heparins (LMWH) such as enoxaparin (4 kDa - 6.5 kDa) which offer once-daily dosing without need of monitoring and demonstrate consistent pharmacokinetic after subcutaneous administration for the treatment of deep vein thrombosis (Bai, et al. 2022; DeBiase, et al. 2021; Veeranki, et al. 2021). Common doses of LMWH appear insufficient for preventing venous thromboembolism in COVID-19 patients, as significantly higher doses of anticoagulant are required to achieve the necessary target Anti-Xa concentration (Watson, et al. 2023). Sulfated polysaccharides have demonstrated the ability to prevent or treat SARS-CoV-2 by limiting viral entry through the spike protein's interaction with cell surface glycosaminoglycans, thereby preventing it from binding to the angiotensin-converting enzyme-2 (ACE-2). Additionally, heparin can inhibit the SARS-CoV-2 main proteinase (Ballacchino, et al.), an essential enzyme for viral replication. Their unique structural

characteristics, including negatively charged sulfate groups, enable them to interact with the Mpro active site, leading to its inhibition. Furthermore, sulfated polysaccharides exhibit antibacterial, non-anticoagulant, anti-inflammatory, and potential effects on cancer diseases (Clausen, et al. 2020; Feng, et al. 2023; Jabeen, et al. 2021; Lu, et al. 2021; Ruiz, et al. 2022).

The efficacy of inhalation of enoxaparin as a nebulizer prophylaxis treatment against SARS-CoV-2 virus was investigated by Eder et al. (2022), demonstrating excellent results in its capacity to halt virus propagation (Eder, et al. 2022). Additionally, pretreating Vero E6 cells and normal human bronchial epithelial (NHBE) cells with enoxaparin showed a prophylactic effect, preventing infection. However, the duration of the protection from the virus after inhaling enoxaparin has not been established.

AZM is extensively used to treat pulmonary infections due to its ability to accumulate in lung tissues and immune cells after oral administration within a short course (2 days). AZM is the first-line treatment for mild-to-moderate community-acquired pneumonia caused by common respiratory bacteria, as it reduces exacerbation frequency and improves lung function in chronic respiratory disorders such as cystic fibrosis and non-cystic fibrosis bronchiectasis. AZM is also used during acute exacerbations of COPD. In COVID-19 patients, AZM has been employed for its antiviral and anti-inflammatory effects (Albert, et al. 2011; Leal, et al. 2016; Oliver and Hinks 2021). AZM has recently emerged as a promising candidate for inhaled therapy due to its potential to effectively treat lung infections while limiting systemic side effects. In children with HIV-associated chronic lung disease, AZM has demonstrated benefits in reducing acute respiratory exacerbations, although it did not significantly improve lung function or growth (Ferrand, et al. 2020). AZM-loaded in albumin microspheres exhibited a mean geometric size of 10 μm, which was not suitable for dry powder inhalers (DPIs). However, after intravenous administration, a preferential accumulation in the lung parenchyma was observed (Ramaiah, et al. 2016).

To enhance lung deposition, DPIs have been developed as a convenient and efficient platform for pulmonary drug delivery, offering improved stability, patient compliance, and targeted lung deposition (1 μm – 5 μm). DPIs are promising for targeting bacterial pneumonia and respiratory illnesses, such as COVID-19 (D'Angelo, et al. 2023; de Pablo, et al. 2023). They focus on the primary infection site in the lungs, enhancing local drug concentrations and reducing systemic exposure. DPI formulations can sustain drug release kinetics and co-deliver multiple drugs, enabling fixed-dose combination therapy (de Boer, et al. 2017). However, particle engineering is crucial in ensuring successful drug delivery to the lung. Currently, it remains poorly understood how sulfated polysaccharides can be utilized as vehicles for lung delivery in combination with antibiotics to exert enhanced activity against lung infections.

The hypothesis driving this research is that developing DPI formulations combining heparin or its derivatives with AZM could provide a comprehensive response to pathogenic processes in the lung associated with bacterial pulmonary infections associated with COVID-19. By

simultaneously co-administering and delivering both molecules to the lung parenchyma, a combined effect encompassing antiviral, antibacterial, immunomodulatory, anti-coagulant, and anti-inflammatory effects can be achieved. For the first time, microparticle engineering for lung co-delivery of heparin or its derivatives, specifically enoxaparin, loaded with AZM will be developed. Additionally, the investigation seeks to explore the physicochemical properties, biocompatibility, and antibacterial and antiviral efficacy against COVID-19 of the developed novel formulations.

2. Materials and methods

2.1. Materials

Heparin sodium salt (purity > 95 %), CAS # 9041-08-1 from porcine intestinal mucosa, Lot No. A0411030 (203.5 IU/mg, Acros organics) was purchased from Fisher Scientific (Madrid, Spain). AZM with purity ≥ 95 % was bought from Kemprotec (Cumbria, UK), and leucine with purity ≥ 98 % was purchased from Sigma Aldrich (Madrid, Spain). Enoxaparin sodium (Clexane 40 mg/0.4 mL) was purchased from Sanofi (Madrid, Spain). The solvents of HPLC grade were used. All other chemicals were of reagent grade and were used without further purification.

2.2. Methods

2.2.1. Design of experiments (Jones, et al.): Defining the target product profile (TPP) and identifying the critical quality attributes (CQAs)

TPPs guide the development of prototypes to meet user requirements for DPIs. The TPP includes drug quality, efficacy, and safety considerations, dosage form, route of administration, dosage type, pharmacokinetics, packaging, and stability. In this study, optimization of a pulmonary DPI formulation focused on achieving a suitable aerodynamic particle size to reach the lung (1 µm - 5 µm) and ensure adequate entrapment of AZM within heparin microparticles. CQAs such as spray drying yield, encapsulation efficiency, and geometric particle size play a pivotal role in defining the TPP (de Pablo, et al. 2023).

2.2.2. DoE studies

DPI comprising heparin sodium ranging from 75 % to 95 %, with a fixed AZM loading of 5 % w/w, and leucine to enhance flow properties ranging from 0 % *w/w* to 20 % *w/w* were studied. A DoE study utilizing a three-factor eight-run design at two levels ($L2^3$) was employed to identify the formulation and process variables significantly impacting product quality. The software Design Expert® version 10.0 (M/s Stat-Ease, Minneapolis, USA) was used to develop polynomial models, which were analyzed to delineate the main effects for each Critical Quality Attribute (CQA) via Pareto charts. Two factors with three levels each affecting DPI formulation development were selected. Each factor was numerical: **(1)** Air flow rate: 500 NL/h or 800 NL/h; **(2)** Solution feed rate: 5 % or 20%, equivalent to 2.5 mL/min or 10 mL/min; and **(3)** Leucine content: 0 % or 20% *w/w*. The AZM amount was

fixed at 5 % *w/w*, and the heparin amount was adjusted to up to 100 % based on the leucine content as per the DoE matrix design.

A total of eight formulations were prepared (**Table 1**). The spray-dried powders were obtained from a water solution containing 10 % (*w/v*) solids in a Büchi B191 Mini Spray Dryer (Büchi Labortechnik AG, Switzerland) equipped with a high-efficiency cyclone in open mode. The process parameters were set as follows: inlet temperature was set to 150 °C, the solution feed rate was set to 2.5 mL/min or 10 mL/min (equivalent to 5 % or 20% *w/w*), the airflow rate to 500 NL/h or 800 NL/h, and the aspirator force to 95 % (equivalent to 28 m^3/h). Under these conditions, an outlet temperature of 80 ºC – 87 ºC was recorded. Four responses were evaluated for collected particles: yield, geometric particle size, AZM loading efficiency, and encapsulation efficiency.

The yield was calculated by considering the difference in weight between the dry powder collected after the spray drying process and the total weight of solutes (excipients and Active Pharmaceutical Ingredients) introduced into the feed solution, using the following **Equation (1).**

$$\text{Yield (\%)} = \frac{\text{Weight of collected spray-dried formulation}}{\text{Weight of solutes in the feed solution}} 100 \quad \textbf{(1)}$$

The geometric particle size distribution was determined by laser diffraction using a Malvern®-Mastersizer 2000 (Malvern Instruments Ltd., Worcestershire, UK). Powder formulations were dispersed using a Scirocco dry feeder instrument with 3 bar pressure and a vibration feed rate of 75 % to achieve an obscuration of 0.5 % – 3 %. The results were reported as the median particle size (D_{50}).

High-performance liquid chromatography (HPLC) analysis was conducted using a modular Jasco equipment setup comprising a Jasco PU-1580 pump, a Jasco AS-2050-Plus autosampler equipped with a 100 µL sampling loop, and a UV-visible detector Jasco UV-1575. AZM was separated on a Thermo Scientific BDS Hypersil C18 reverse-phase column (250 mm × 4.6 mm, 5 µm). A previously validated HPLC method for AZM - was employed with a mobile phase consisting of phosphate buffer (0.2 M KH_2PO_4, pH 8): methanol (1:10 *v/v*) (Al-Hakkani 2019). The mobile phase was filtered through a hydrophilic 0.45 µm filter (Millipore, Millex-LCR, Merck, Madrid, Spain), and pumped at a flow rate of 1.2 mL/min. The sample injection volume was 50 µL. The column temperature was maintained at room temperature, and the detector was set at 210 nm.

For drug loading (DL) and encapsulation efficiency (EE) quantification, approximately 5 mg of each powder formulation (n = 3) from each DoE run was weighed and dispersed in 1 mL of the mobile phase. The sample was then sonicated and vortexed for 5 min before being centrifuged for 5 min at 5,000 rpm. The supernatant was subsequently analyzed by HPLC. AZM concentrations were determined by integrating the peak area at 4.5 min using a

calibration curve. DL was calculated using **Equation (2)** and, EE using **Equation (3)**, both expressed as a percentage:

$$\mathrm{DL}\ (\%) = \frac{(\text{Concentration of active ingredient in the powder})\ \text{Volume}}{\text{weight of powder formulation}} 100 \quad \textbf{(2)}$$

$$\mathrm{EE}\ (\%) = \frac{\text{Total drug encapsulated}}{\text{Total drug content}} 100 \quad \textbf{(3)}$$

2.2.3. Optimisation of DPI formulations and validation studies

Mathematical modelling was conducted using multiple linear regression analysis. The polynomial equations were derived from statistically significant coefficients ($p < 0.05$). The correlation coefficient (R^2) and predicted residual sum of squares were used to assess the models. Response surface analysis was performed using 3D plots to elucidate the relationship between various factors and responses. Optimum formulations were predicted through numerical optimization and desirability function. Validation of the Quality by Design (QbD) methodology was accomplished by comparing predicted responses with experimental ones, supported by linear correlation and residual plots.

Morphology and particle size characterization

The mean particle size after dispersion in aqueous media (5 mg/mL), polydispersity, and zeta potential were measured using a Zetasizer (Malvern Instruments, Malvern, UK). Measurements of mean particle size and polydispersity were performed at a scattering angle of 90º and a temperature of 25 ºC. Prior to measurements, polystyrene standards (diameter = 100 nm) were measured; size results were in accordance with the nominal size of the standard particles.

Transmission Electron Microscope (TEM) (JEM 1400 plus JEOL, Japan) equipped with an acceleration voltage ranging from 40 kV to 120 kV was used for imaging. A drop of an aqueous sample dispersion (5 mg/mL) was placed onto a Formvar/carbon-coated grid, and the excess sample was blotted off with the Whatman Nº 1 filter paper. The samples were then negatively stained with 1 % *w/v* phosphotungstic acid solution. Images were captured using an AMT digital camera (Smith, et al. 2018).

2.2.4. Solid state characterization

Morphology

The morphology of the optimized microparticulate formulations was characterized by Scanning Electron Microscopy (SEM) (JSM 6335F JEOL, Japan) equipped with a secondary electron detector at 15 kV. Samples were sputter coated with pure gold using a metallizer (Q150RS Metalizador QUORUM, Quorum Technologies Ltd., Lewes, UK) for 180 s under vacuum.

Powder X-Ray Diffraction (pRXD)

Powder X-ray analysis was conducted using a Philips®X'Pert-MPD X-ray diffractometer (Malvern Panalytical®; Almelo, The Netherlands) equipped with Ni-filtered Cu K radiation (1.54). The study was performed at 40 kV voltage and 40 mA. PXRD patterns were recorded at a step scan rate of 0.05°/s, ranging from 5° to 40° on the 2-theta scale (n = 3). For comparison purposes, physical mixtures of raw powder materials between API and excipients, prepared in an agate mortar and pestle were used.

Fourier-Transform Infrared (FTIR) Spectroscopy

FTIR analysis was performed using a Nicolet Nexus 670–870 (Thermofisher, Madrid, Spain). A wavelength range between 400 cm^{-1} – 4000 cm^{-1} was used with a 1 nm step scan. Spectra were interpreted using Spectragryph (version 1.2.9, Oberstdorf, Germany) software, and data normalization was carried out.

Differential Scanning Calorimetry (DSC) coupled with a Thermogravimetric Analysis (TGA)

DSC-TGA standard scans were conducted using 4-6 mg weight powder with nitrogen as the purge gas on an SDT Q600 instrument (TA instruments, Elstree, UK) calorimeter. A scanning rate of 10 °C/min was used from 25 °C to 350 °C. The instrument was calibrated using indium as the standard. The glass transition temperatures reported are the midpoint of the transition (n = 3).

Stability studies

The AZM-loaded microparticles (5 mg) were placed in HPLC vials and introduced into test Cuspor stability chambers exposed to different conditions of temperature corresponding to refrigerated (4 °C ± 2 °C) and room temperature (25 °C ± 3 °C) conditions. A sensor cap was introduced to the test chamber to collect the temperature test conditions wirelessly. Samples were collected and analyzed by HPLC for chemical degradation at 6 months.

2.2.5. *In vitro* Haemolysis Assay

Haemolysis studies were performed with red blood cells (RBCs) to assess the toxicity of the formulation. Cells were obtained from the blood of a healthy 28-year-old male volunteer, following ethical procedures approved by Universidad Complutense de Madrid (Madrid, Spain) in EDTA coated Vacutainers® (K2-EDTA, BD Vacutainer® tubes, Becton Dickinson and Co., New Jersey, USA). The blood was centrifuged at 3,000 rpm for 5 min, and hematocrit and plasma levels were marked on the tube. The supernatant (plasma) was removed, and the erythrocytes were washed three times with an equivalent volume of 0.9 % NaCl (150 mM), followed by centrifugation at 3,000 rpm for 5 min at each step. After washing, the supernatant was discarded, and the RBCs were resuspended in PBS pH 7.4 to a final concentration of 4 % *w/w*. Subsequently, a volume of 180 µL was added to each well (Pineros, et al. 2017). Samples (microparticles, excipients, and APIs) were dispersed with PBS (1X, pH 7.4) to produce a final AZM concentration of 200 µg/mL, 100 µg/mL, 50

μg/mL, 25 μg/mL, 12.5 μg/mL, 6.25 μg/mL, 3.125 μg/mL and 1.65 μg/mL (20 μL, *n=3*). Triton® X-100 (Sigma-Aldrich CO, St. Louis, USA) in PBS (1X, pH 7.4) prepared at 20% *w/v* or PBS (1X, pH 7.4) were used as a positive and negative control (20 μL) respectively. The plates were then incubated at 37 ºC for 1 h (Memmert GmBH + Co., Schwabach, Germany). Subsequently, the plates were centrifuged at 1,500 rpm for 5 min to pellet intact erythrocytes. The supernatant (100 μL) was transferred to a clear flat-bottomed 96-well plate. Absorbance (ABS) was measured at 570 nm using a plate reader (BioTeK, EKx808). The percentage of haemolysis was calculated using the **Equation (4):**

$$\%\, Hemolisis = \frac{ABS1-ABS2}{ABS3-ABS2}100 \quad \textbf{(4)}$$

where ABS1 sample represents the absorbance of the sample, ABS2 is the absorbance of the negative control, and ABS3 is the absorbance of the positive control. The concentration needed to produce 50 % haemolysis (HC_{50}) was calculated using Compusyn™ v1.0 (Combosyn Inc., New Jersey, USA).

2.2.6. *In vitro* Lung Deposition

A Next Generation Impactor (NGI; Copley Scientific, Nottingham, UK), connected to an SCP5 vacuum pump (Copley Scientific, Nottingham, UK) through a critical flow controller (TPK Copley Scientific, Nottingham, UK) was used. The NGI apparatus comprised seven stainless compartments (stages), a stainless-steel induction port, and one micro-orifice collector (Annisa, et al.). To ensure accurate analysis and prevent particle bouncing, the cups of the impactor were coated with a solution of 2 % (*w/v*) Tween 20 in ethanol and led the solvent to evaporate before use. Airflow of 60 L/min was set using a DFM 2000 Flow Meter (Copley Scientific, UK), with an inhalation time of 4 s and a total inhaled air volume of 4 L. For the aerosolization, a hydroxypropyl methylcellulose capsule (No. 3) filled with 25 mg ± 1 mg of formulation (n = 3) was placed in a RS01 (Plastiape, Lecco, Italy) device. The formulations deposited in each part of the NGI were quantified using the previously described HPLC method. The mass median aerodynamic diameter (MMAD) and fine particle fraction (FPF) (<3 μm and <5 μm) were calculated to evaluate the *in vitro* deposition of the tested formulations, as per established protocols (D'Angelo, et al. 2023; de Pablo, et al. 2023). Aerodynamic cut-off diameters at the flow rate used were as follows: 8.06 μm, 4.46 μm, 2.82 μm, 1.66 μm, 0.94 μm, 0.55 μm, 0.34 μm from stage 1 to stage 7, and <0.34 μm to MOC, respectively (Wong, et al. 2022).

2.2.7. Microbiological *in vitro* Assays

2.2.7.1. Pseudovirus neutralization assay against SARS-CoV-2

The pseudovirus neutralization of the formulations was tested against 293T cell line (C-HA101) overexpressing the hACE2 receptor and hTMPRSS2 on the surface (COVID-19 Coronavirus Receptor Stable Cell Lines, 2024). These cells were cultured in advanced Dulbecco Modified Eagle Medium (DMEM) supplemented with 10 % *v/v* Fetal Bovine

Serum (FBS), 1 % *v/v* of penicillin/streptomycin, and 10µM HEPES. A stock solution for each formulation was prepared at 1 mg/mL and further diluted (1:4 *v/v*) with media. A Variant Omicron BA.2 (Lot: 220811SLVB33; Preclinics GmbH, Wetzlarer Str. 20, D-14482 Potsdam) was used. The undiluted virus (15 µL) was diluted with 2385 µL of media. The neutralization assay was conducted following the manufacturer's protocols. Briefly, 8-fold serially diluted formulations (45 µL) were incubated with the pseudotyped SARS-CoV-2-luciferase (45 µL) for 1 h at 37 °C. The mixtures (90 µL) were then incubated with 293T-hsACE2 cells at 0.2 x 10^6 cells/mL in a 384-well Corning white (80 µL). Infection was established and validated for 72 h at 37 °C with 5 % CO_2. The luciferase signal was measured using the *Renilla*-Glo luciferase assay system (Promega, Cat# E2720) with a luminometer at 5 s integration time. The obtained relative fluorescent/luminescence signals (RFU/RLU) from the negative control wells were normalized, and the neutralization percentage for each concentration was calculated. Data was analised using Origin 2021 (OriginLab Corporation, Northampton, MA, USA) to fit into a 4PL curve and to calculate the logIC_{50} (half-maximal inhibitory concentration). 293T cells incubated with pseudoviruses alone without formulation served as the positive control (maximum infectivity), while pseudovirus in culture media without formulation was used as a negative control (Xiang, et al. 2020).

2.2.7.2. Antibacterial *in vitro* Assay

The activity of the formulations was assessed against *Streptococcus pneumoniae* (NCTC 12977) and *Pseudomonas aeruginosa* (CECT 110), obtained from the Collection Española de Cepas (Valencia-Spain). The minimum inhibitory concentration (MIC) was determined using the broth microdilution method in a 96-well plate (n = 3), following the guidelines of the Clinical Laboratory Standards Institute (guidelines) (guidelines). AZM stock solutions were prepared at a concentration of 500 µg/mL. Twelve serial dilutions (1:1 *v/v*) using Mueller-Hinton Broth (MHB) medium were tested. Formulations were dispersed at equivalent AZM concentrations.

Cultures were separated from the culture medium by centrifugation (3,000 rpm) for 5 min. The supernatant was discarded, and cultures were washed, resuspended, and diluted with saline solution (0.9 %) to achieve an optical density of 0.5 McFarland units at 600 nm. Subsequently, 100 µL of the bacterial suspension (equivalent to a concentration of 5×10^5 colony forming units (CFU/mL) was added to each well of the 96-well plate, and mixed with 100 µL of each AZM stock concentration. The plates were then incubated at 37 ºC for 18-20 h. The sterile broth was used as the negative control, while the inoculated broth without AZM was used as the growth-positive control. Antimicrobial growth was determined by monitoring the optical density at 600 nm using a microplate reader (VictorTM X3, 2030 Multilabel Reader, Perkin Elmer). The lowest concentration without turbidity was considered as the MIC. To determine the Minimum Bactericidal Concentration (MBC), 100 µL of the culture media was plated on Mueller-Hinton agar (MHA) and incubated at 37 ºC over 18 h.

The lowest concentration that did not exhibit any bacterial growth was considered as the MBC.

2.2.9. *In vitro* cell culture assays

Cell Culture Conditions

Human bronchial epithelial Calu-3 cells, obtained from ATCC (No. HTB-55, Lot. 61449062), were cultured in DMEM/F-12 with glutamine supplemented with 10 % Fetal Bovine Serum (FBS) and 1 % penicillin/streptomycin. Murine macrophage J774A.1 cells (ATCC® TIB-67™) were cultured in RPMI-1640 medium supplemented with 10 % FBS and 1 % penicillin/streptomycin. The cells were maintained at 37 ºC in a humidified incubator with 5 % CO_2.

Cell Viability Assay

MTT assay was used to assess cell viability. Cells were seeded in 96-well culture plates at a density of 3.0×10^4 cells per well (Calu-3 cells) and 1.0×10^4 cells per well (J774A.1 cells). Calu-3 cells were treated with different concentrations of AZM ranging from 0.10 µg/mL to 50 µg/mL for 24 h. J774A.1 cells were pre-treated with AZM (concentrations from 0.10 µg/mL to 50 µg/mL for 1 h) following by lipopolysaccharide (LPS) treatment (1 µg/ml for 24 h). Triton-X solution (5 %) was used as a negative control. After treatments, MTT solution (5 mg/mL) was added (100 µL), and cells were incubated for 4 h in the darkness. Formed formazan crystals were then dissolved in isopropyl alcohol (Calu-3 cells) or DMSO (J774A.1 cells). Absorbance was measured at 550 nm using a Spectrostar BMG microplate reader. (BMG LABTECH, Ortenberg, Germany). The percentage of viable cells was calculated using untreated cells as control, being considered as 100 % cell viability. MTT assays were done in triplicate.

Nitric oxide determination

J774A.1 cells were pretreated with AZM (from 0.10 µg/mL to 50 µg/mL) for 1 h, and then treated with LPS (1 µg/ml) for 24 h. After treatments, supernatant was harvested, and nitric oxide (NO) production was determined based on Griess reaction. Equal volumes of culture medium supernatant from each well (100 µL) were mixed with 100 µL of Griess reagent (2 % sulphanilamide + 2 % naphthylene-diamide dihydrochloride in 10 % H_3PO_4) at room temperature. The spectrophotometric absorbance was read at 550 nm wavelength.

2.2.8. Statistical Analysis

Statistical analysis was performed via a one-way ANOVA test using Minitab v.17 (Minitab Ltd., Coventry, UK) followed by Tukey's test (95 % level of significance). The results were plotted using Origin 2021 (OriginLab Corporation, Northampton, MA, USA).

3. Results

3.1. DoE and DPI Formulation Optimization

The factors and responses evaluated in the DoE are shown in **Table 1**. To understand the influence of each factor on the dependent variables, three-dimensional (3D) surface response, and Pareto charts were constructed (**Figure 1**). The analysis of the 3D surface plots revealed that the solution feed rate (pump) and the airflow significantly affected the yield (**Figure 1A**). The higher the pump, the lower the yield while the opposite correlation was observed for the airflow. Regarding particle size, only airflow demonstrated a significant effect (**Figure 1B**). The greater the airflow, the lower the particle size of the microparticles. However, neither the airflow nor the pump showed a significant effect on the AZM encapsulation efficiency within the microparticulate formulation. In this case, only leucine demonstrated a significant correlation with AZM encapsulation efficiency. The higher leucine content in the formulation resulted in greater AZM encapsulation efficiency (**Figure 1C**).

Table 1. DoE matrix including dependent and independent factors.

Run	Airflow (NL/h)	Pump (%)	Leucine (%)	Yield (%)	Particle Size (µm)	AZM Encapsulation (%)
1	500	5	0	24	6.28	21
2	500	20	20	16	3.67	89
3	500	20	0	13	5.58	25
4	500	5	20	44	5.45	87
5	800	20	0	42	3.53	31
6	800	5	20	60	3.31	76
7	800	20	20	39	3.10	86
8	800	5	0	70	3.42	29

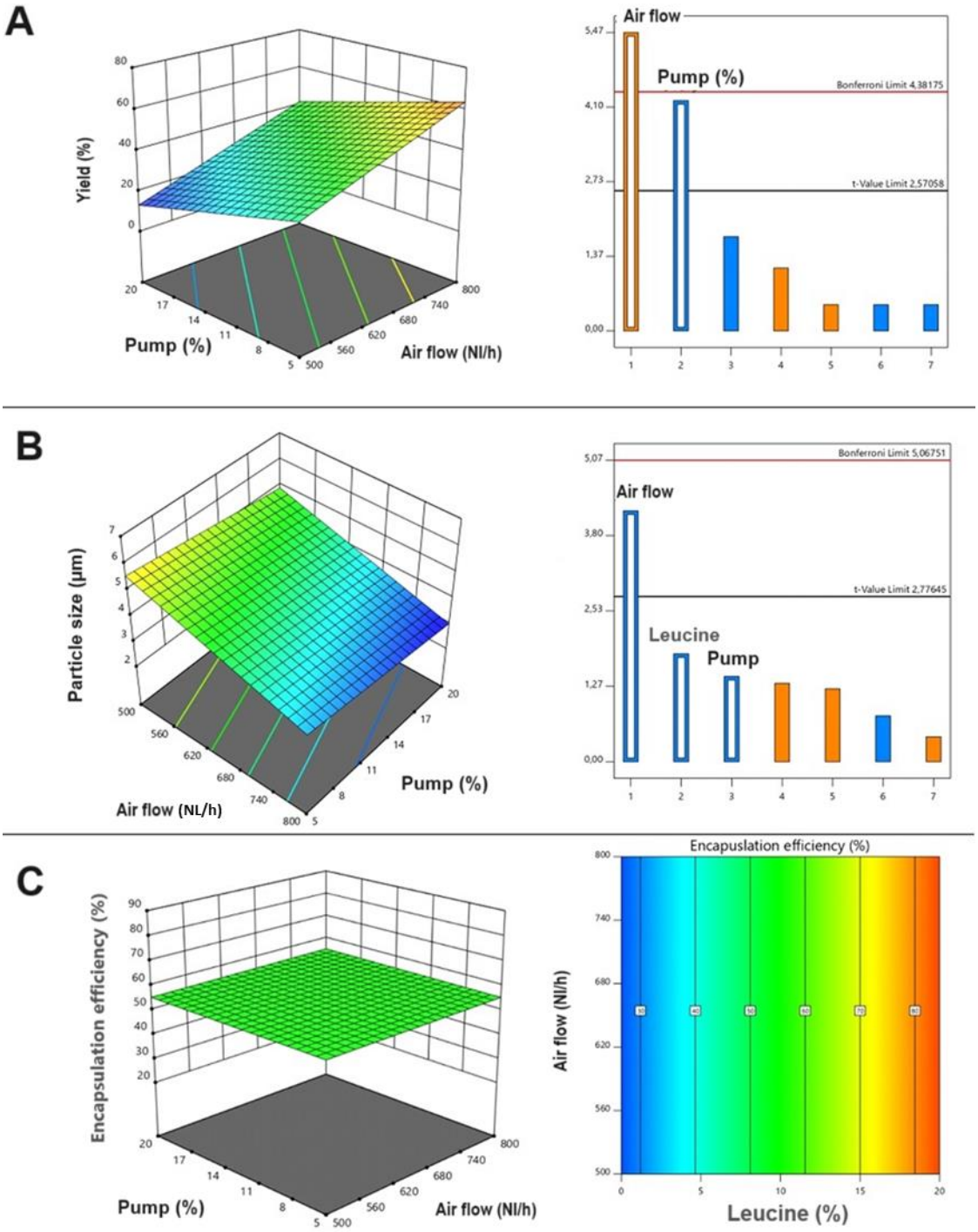

Figure 1. **Influence of the factors (pump, airflow, and leucine content) in the DoE design**. Key: **(A)** Impact of the factors on the yield (%), **(B)** Impact of the factors on the particle size (µm), and **(C)** Impact of the factors on the encapsulation efficiency (%).

Based on the DoE, the critical attributes affecting the spray drying process were identified, and optimized to achieve the highest yield and drug encapsulation, while minimizing the geometric particle size. The optimized formulation consisted of 75 % heparin, 5 % AZM and

20 % leucine, using an airflow rate of 800 NL/h, a solution feed rate of 5 % (equivalent to 2.5 mL/min), an inlet temperature of 150 °C, and aspiration rate of 95 %.

Additionally, using the optimized parameters described, two formulations were developed. In the first formulation, heparine was replaced with enoxaparin sodium to evaluate the impact of LMWH. The second formulation contained the same percentage of excipients, but the total solid concentration before spray drying was reduced to 1% instead of 10% to evaluate the impact on the particle characteristics (**Table 2**).

The CQAs of the three optimized above described formulations are summarised in **Table 2**. In the case of the heparin formulations (Rehfeld, et al.), the percentage of solids before spray drying affect the median geometric particle size (D_{50}) which ranged from 3.32 µm to 1.66 µm. This indicates the impact of the total solid content in the solution before spray drying on the final geometrical particle size. Adjusting the total solid content in the solution, the final particle size of the microparticles in a dry state was controlled. A similar trend was observed for the AZM encapsulation efficiency and lower solid content in the solution favored the drug encapsulation but negatively impacted on the yield. Heparin formulation spray dried from a 10 % solid content in the solution (HF10%) exhibit significantly higher yield compared to HF1% (heparin formulation spray dried from a 1 % solid content in the solution). However, no statistical differences were observed between heparin and its derivative (enoxaparin).

Table 2. CQAs of the three optimised formulations. Key: **(HF10%)** Heparin formulation containing 10% (*w/v*) solids, **(HF1%)** Heparin formulation containing 1% (*w/v*) solids, and **(EF10%)** Enoxaparin formulation containing 10% (*w/v*) solids before spray drying. For AZM encapsulation and yield, it is reported in the brackets the lowest and the highest value obtained.

Formulation	Yield (%)	Particle Size D_{50} (µm) (D_{10}-D_{90})	AZM Encapsulation Efficiency (%)
HF10%	67.8 (65 - 70)	3.5 (1.9 - 6.2)	74 (72 - 78)
HF1%	55.0 (40 - 60)	1.7 (0.9 - 3.4)	86 (83 - 89)
EF10%	64.3 (56 - 72)	3.3 (1.8 - 5.9)	84 (76 - 86)

Leucine was incorporated in the formulation as can act as a dispersibility enhancer and surface modifier during the spray-drying process. Its amphiphilic nature allows it to migrate to the surface of the drying droplets, forming a hydrophobic coating that reduces particle cohesion and improves powder dispersibility (Molina, et al. 2018; Vehring 2008). The high encapsulation efficiencies observed, particularly in the HF1% and EF10% formulations, can be attributed to surface modification, resulting in AZM encapsulation rates of 86 % and 84 %, respectively (**Table 2**).

Long-term stability studies showed optimal chemical stability for HF1% and EF10% for 6 months when stored under refrigerated conditions (> 90 % AZM content), while HF10% showed a poorer stability profile for AZM. The amorphous nature of AZM was maintained over this period; however, Bragg peaks attributed to leucine were clearly obrserved in all

three formulations which may impact it aerodynamic deposition pattern being required to use a specific dry power inhaler device to prevent from moisture (**Figure S1, supplementary material**).

3.2.Morphological Evaluation

SEM micrographs displayed the particle morphology of the three optimised formulations after spray drying (**Figure 2**). No crystals were observed in any of the micrographs, indicating the full entrapment of AZM within the microparticles. The latter showed a corrugated appearance for all three formulations with a bimodal distribution. However, the surface of HF10% microparticles showed a more pronounced angular surface compared to HF1%. This angular surface was only observed in the largest particles above 1 µm compared to the smooth surface presented by the smallest ones. In the case of HF1% and EF10%, particles exhibited a corrugated surface which was related to the fast evaporation rate of the process.

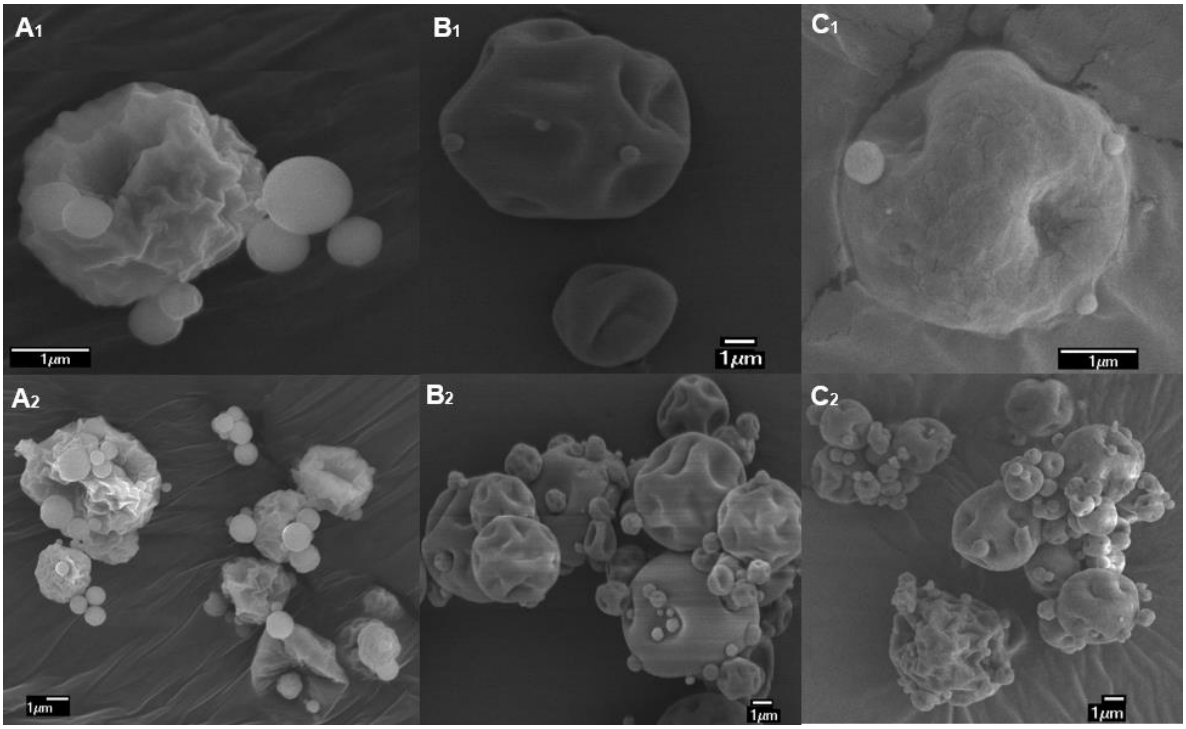

Figure 2. Morphological analysis of optimised formulations. SEM micrographs were obtained at different magnifications. Key: **(A1, A2)** HF10%; **(B1, B2)** HF1%, and **(C1, C2)** EF10%.

The particle size after reconstitution of microparticles in aqueous media ranged between 500 to 3,000 nm in all three formulations (**Figure 3**) and particles showed a negative zeta potential below -20 mV for all of them indicating good colloidal stability. Electron dense particles above 1 µm in size were observed using TEM (**Figure 3**).

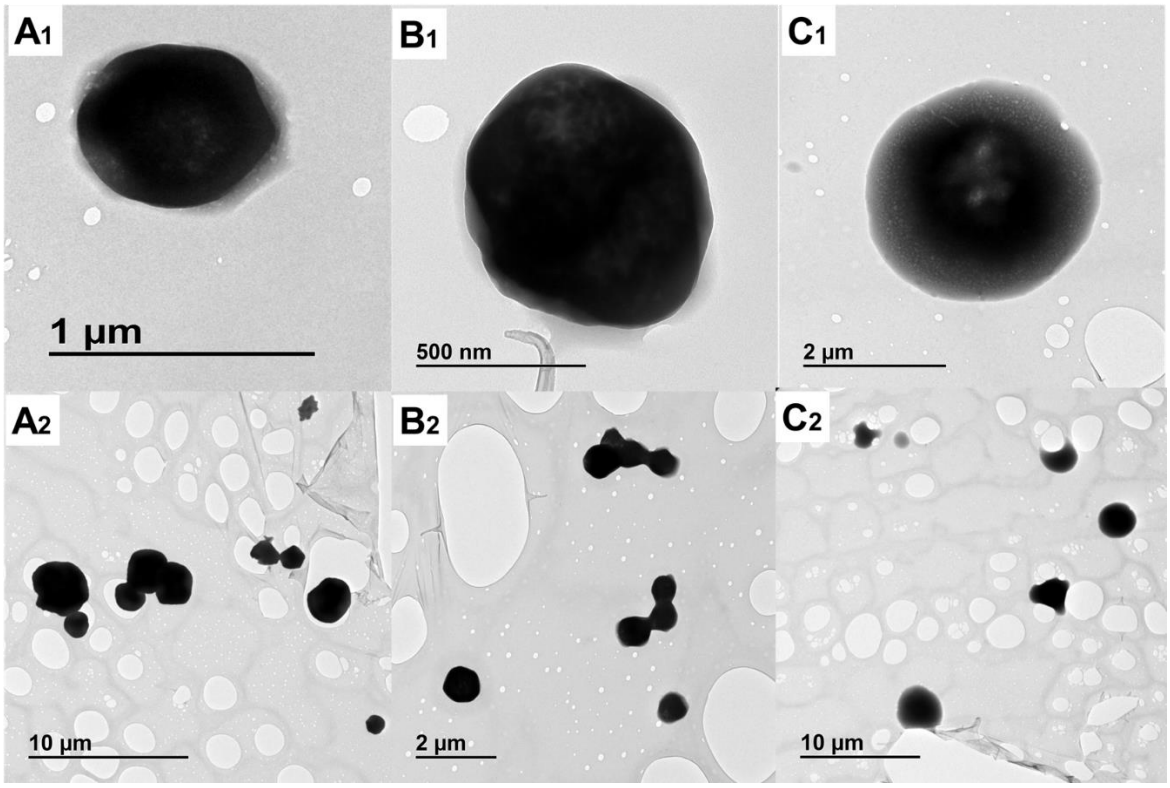

Figure 3. Morphological evaluation of optimised formulations. TEM micrographs were obtained at different magnifications. Key: **(A1, A2)** HF10%; **(B1, B2)** HF1%, and **(C1, C2)** EF10%.

3.3. Solid state characterization of optimized formulations

PRXD and FT-IR analysis

The pXRD analysis of unprocessed heparin and enoxaparin showed a characteristic amorphous halo, while leucine and AZM displayed characteristic Bragg peaks (**Figure 4A**). The physical mixtures showed peaks attributed to AZM and leucine. However, the intensity of the Bragg peaks was significantly diminished after spray drying. Both HF10% and EF10% formulations showed peaks attributed to leucine, but no heparin or enoxaparin peaks were detected. An amorphous halo was observed for the HF1%.

FT-IR analysis of HF1% and HF10% and EF10% revealed a shift in the carbonyl stretching vibration band of AZM located at 1719 cm^{-1} (**Figure 4B**). Additionally, the N-H bending vibrations of leucine, typically occurring around 1588 cm^{-1}, also displayed a shift. A broadening of the O-H stretching at 3440 cm^{-1} was observed for the polysaccharides. These shifts are suggestive of the formation of hydrogen bonding interactions between the amino groups of leucine and the sulphate/carboxylate groups of the polysaccharides or the carbonyl groups of AZM. These peak shifts were marked in the formulations compared to the physical mixtures and unprocessed components, provide compelling evidence for the formation of intermolecular hydrogen bonding interactions.

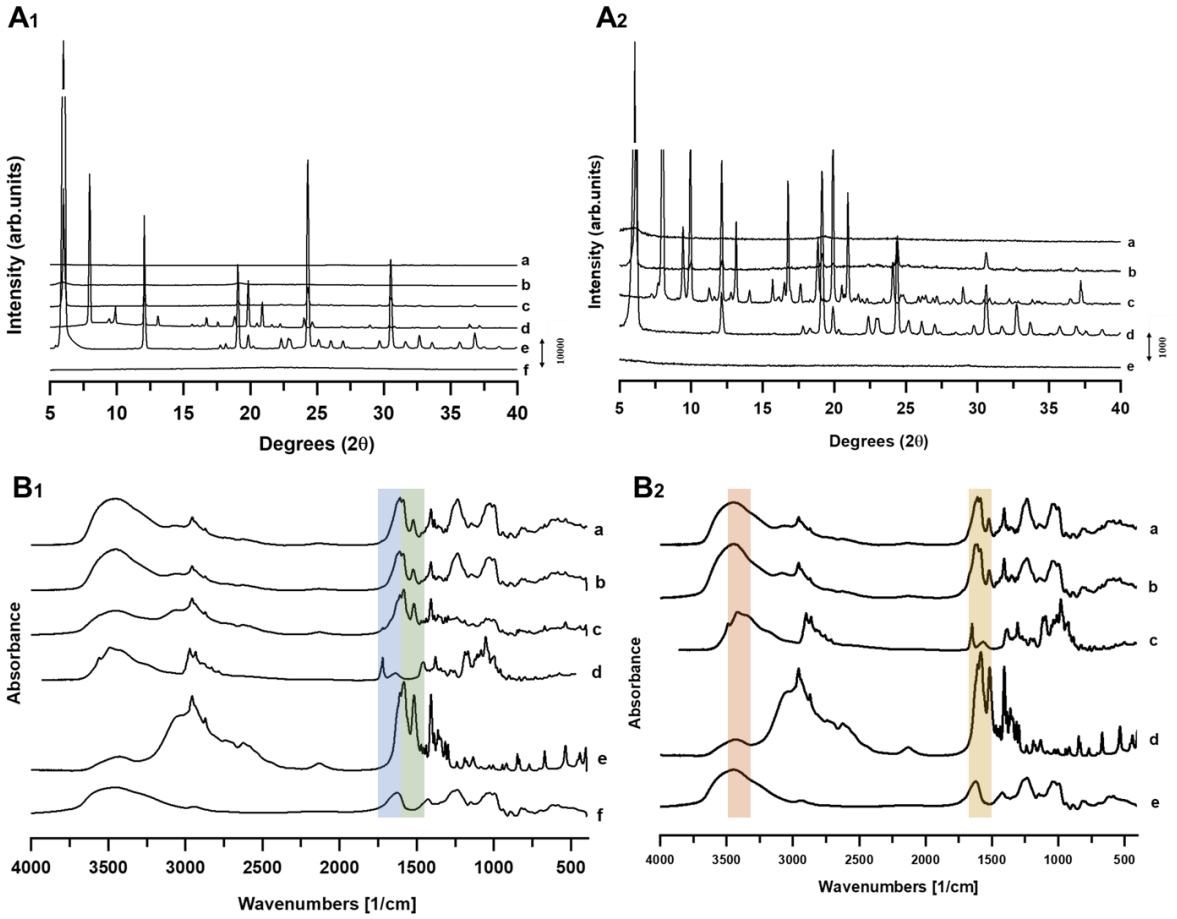

Figure 4. pXRD analysis (A) and FTIR spectra (B). Key: (**A1-B1) (a)** HF1%, **(b)** HF10%, **(c)** Physical mixture, **(d)** Unprocessed AZM, (**e)** Unprocessed leucine, and **(f)** Unprocessed heparin. (**A2-B2)** Key: **(a)** EF10%, **(b)** Physical mixture, **(c)** Unprocessed AZM, **(d)** Unprocessed leucine, and (**e)** Unprocessed enoxaparin.

DSC Analysis

Unprocessed heparin and microparticulate formulations showed a marked dehydration event from 25 ºC to 100 ºC followed by a sharp decomposition peak at around 250 ºC. Despite its amorphous nature in the PXRD analysis, no evidence of a T_g was found, which can be attributed to the overlapping with the dehydration peak. The T_g of undried unprocessed UFH was reported at 50 ºC, while after spray drying, this value was reduced to 38 ºC (Shur, et al. 2008a). In the case of AZM dihydrate, a sharper dehydration peak was observed at 120.4 ºC ± 1.3 ºC, followed by a decomposition peak at similar temperature (**Figure 5**). Similar findings were reported for other authors in literature (Güler and Çallioğlu 2023; Qiu, et al. 2021b). Unprocessed leucine exhibited a very sharp endothermic peak at 287.6 °C ± 0.3°C with a heat of fusion of 901.9 J/g ± 0.1 J/g. TGA analysis demonstrated that leucine is a waterless material and remained stable at temperatures as high as 256 ºC (**Figures 5A2-B2**). AZM-loaded microparticle showed a two steps degradation in the TGA analysis, between

200 ºC and 250 °C, different from the single components, which can be related to the intramolecular hydrogen bonding observed in the FT-IR.

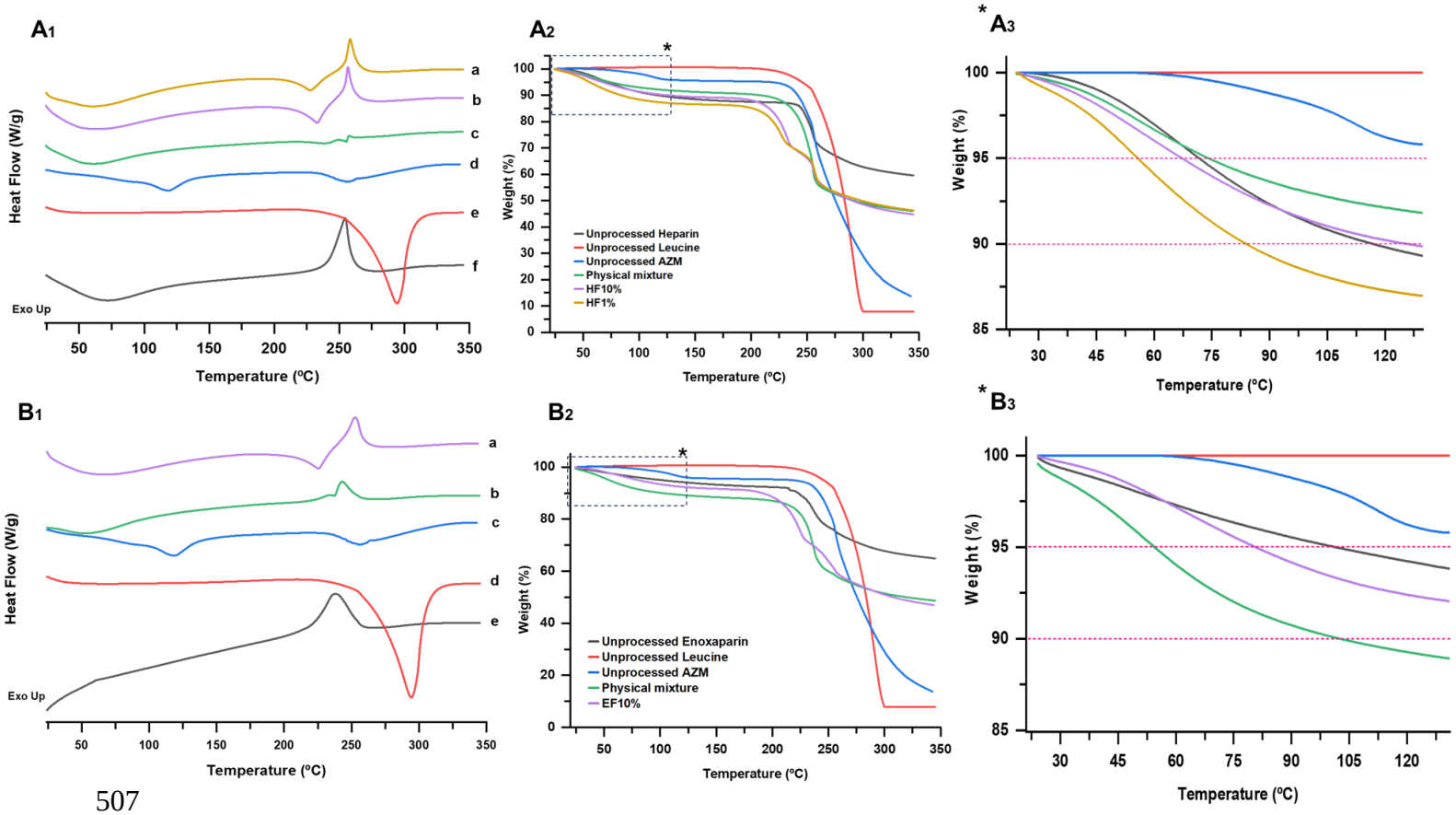

Figure 5. DSC-TGA analysis. **A) Heparin formulations and B) Enoxaparin formulation.** Key: **A1) DSC and A2-3) TGA. (a)** HF1% (Orange) (**-**), **(b)** HF10% (purple) (**-**), **(c)** Physical mixture (green) (**-**), **(d)** Unprocessed AZM (blue) (**-**), **(e)** Unprocessed leucine (red) (**-**), and **(f)** Unprocessed heparin (Troeger, et al.) (**-**). **B1) DSC And B2-3) TGA. (a)** EF10% (purple) (**-**), **(b)** Physical mixture (green) (**-**), **(c)** Unprocessed AZM (blue) (**-**), **(d)** Unprocessed leucine (red) (**-**), and **(e)** Unprocessed enoxaparin (Troeger, et al.) (**-**).

3.4. *In vitro* assessment of aerodynamic performance

The *in vitro* deposition profile of the three formulations is shown in **Figure 6** and summarized in **Table 3**. The percentage of AZM deposited on the different stages of the NGI varied significantly depending on the percentage of solids before spray drying.

Table 3. FPF below 5 µm and 3 µm for HF10%, HF1%, and EF10% at 60 L/min for 4 s. Data are expressed as mean ± SD (n = 3).

Formulation	FPF < 5 µm (%)	FPF < 3 µm (%)	MMAD (µm)
HF10%	31.5 ± 7.1	20.2 ± 11.7	4.4 ± 0.5
HF1%	54.1 ± 3.2	40.5 ± 2.3	1.3 ± 0.1

EF10%	43.8 ± 5.2	31.4 ± 8.1	2.7 ± 0.1

The fine particle fraction (FPF) below 3 µm and 5 µm was significantly higher for HF1% compared to HF10%. As a result, the MMAD of HF1% was 3.4-fold higher than the HF10%. The EF10% showed an intermediate deposition pattern between HF10% and HF1% resulting in an acceptable FPF (**Table 3** and **Figure 6**).

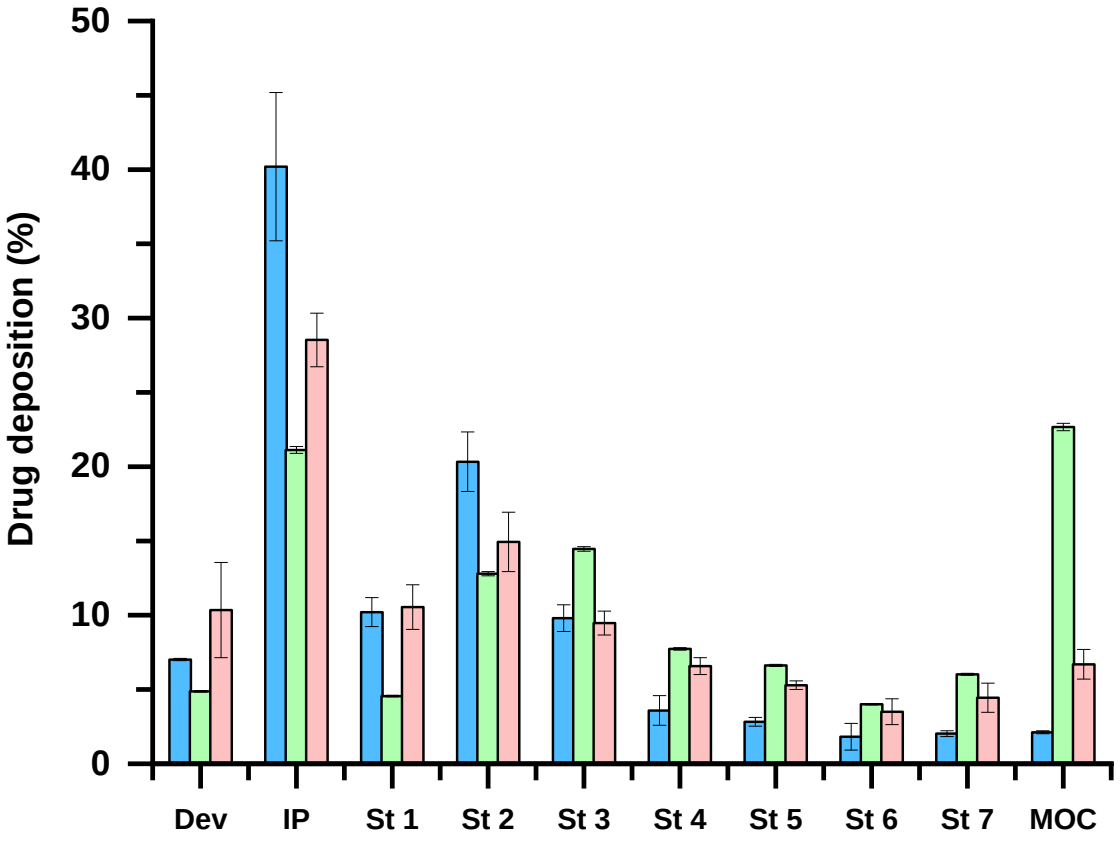

Figure 6. ***In vitro*** **deposition of AZM in different stages of the NGI. Key**: (**Dev)** device + mouce adaptor **(IP)** induction port, **(St)** stage, and (Annisa, et al.) micro-orifice collector. **(a)** HF10% (blue), **(b)** HF1% (green), and **(c)** EF10% (pink orange). Data are expressed as mean ± SD (n = 3).

3.5. Microbiological & Haemolytic *in vitro* assays

Table 4 shows the microbiological efficacy and the *ex vivo* Red Blood Cell (RBC) haemolysis of the AZM formulations. The toxicity against RBCs was compared between the AZM dissolved in PBS pH 7.4 and the microencapsulated AZM. The haemolytic toxicity of the AZM was low, but microencapsulation reduced its toxicity by 10 times, making the heparin-based formulations less toxic than the enoxaparin one. Nonetheless, all the formulations showed less than 5 % haemolysis at 50 µg/mL AZM concentration (**Figure 7A**).

The antibacterial efficacy was tested against *S. pneumoniae* and *P. aeruginosa*, as representatives of Gram-positive and Gram-negative bacteria (Belanger, et al. 2020; Gingras,

et al. 2020). No significant differences ($p > 0.05$) were found between the unprocessed AZM and the formulations against *S. pneumoniae* (**Figure 7C**). However, the AZM encapsulated in microparticles showed a 2 to 4-fold reduction in the MBC for *P. aeruginosa* compared to the free AZM (15.62 µg/mL *vs* 3.90 µg/mL for HF10%) (**Figure 7D**). The neutralization capacity of the pseudovirus was more pronounced when heparin was used as a microparticulate carrier compared to enoxaparin (**Figure 7B**). The concentration needed to neutralize 50 % of the pseudovirus was 13.5 nM and 95.0 nM for heparin and enoxaparin, respectively (**Table 4).**

Table 4. Antimicrobiological (MBC) & *ex vivo* RBC toxicity of AZM DPI formulations. Key: HC_{50}, concentration of AZM that produces 50 % haemolysis at the tested conditions. IC_{50}, concentration of heparin or enoxaparin that causes a 50 % pseudovirus neutralization (Pn). NA, data not available. Data are expressed as mean ± SD (n = 3).

	RBC HC_{50} (10^{7}) (µg/mL)	**Pn IC_{50} (nM)**	**MBC (µg/mL)**	
			S.pneumoniae	***P. aeruginosa***
HF10%	667 ± 62	13.5 ± 3.4	7.81	3.90
HF1%	533 ± 24	NA	7.81	7.81
EF10%	10.5 ± 0.8	95.0 ± 15.6	3.90	7.81
Unprocessed AZM	1.28 ± 0.07	NA	7.81	15.62

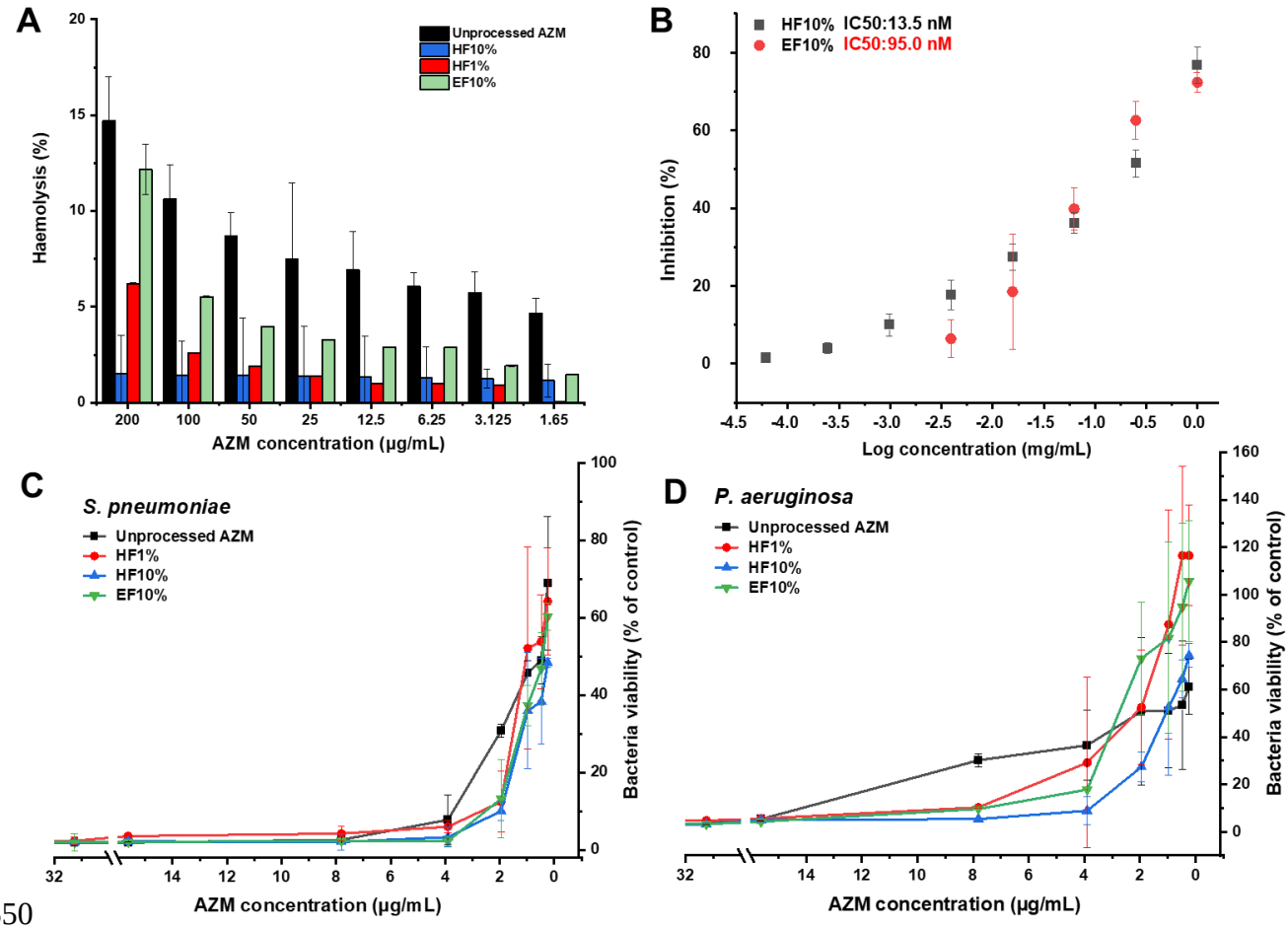

Figure 7. *In vitro* **haemolysis and antimicrobiological efficacy** of AZM formulations. **(A) Haemolysis, (B) Pseudovirus neutralization test** and, **(C & D) Antibacterial Efficacy against *S. penumoniae* and *P. aeruginosa***. Data are expressed as mean ± SD (n = 3).

In vitro cytotoxicity MTT assays

Figure 8 displays the cell viability after 24 h exposure of Calu-3 cells to the AZM formulations, ranging from 50.0 µg/mL to 0.1 µg/mL. Even at the highest concentration tested, no significant differences in cell viability were observed between the AZM formulations and the untreated cells. Cell viability was greater than 90 % in all the AZM concentrations tested. Additionally, no changes in morphology were observed when cells were treated with the AZM formulations.

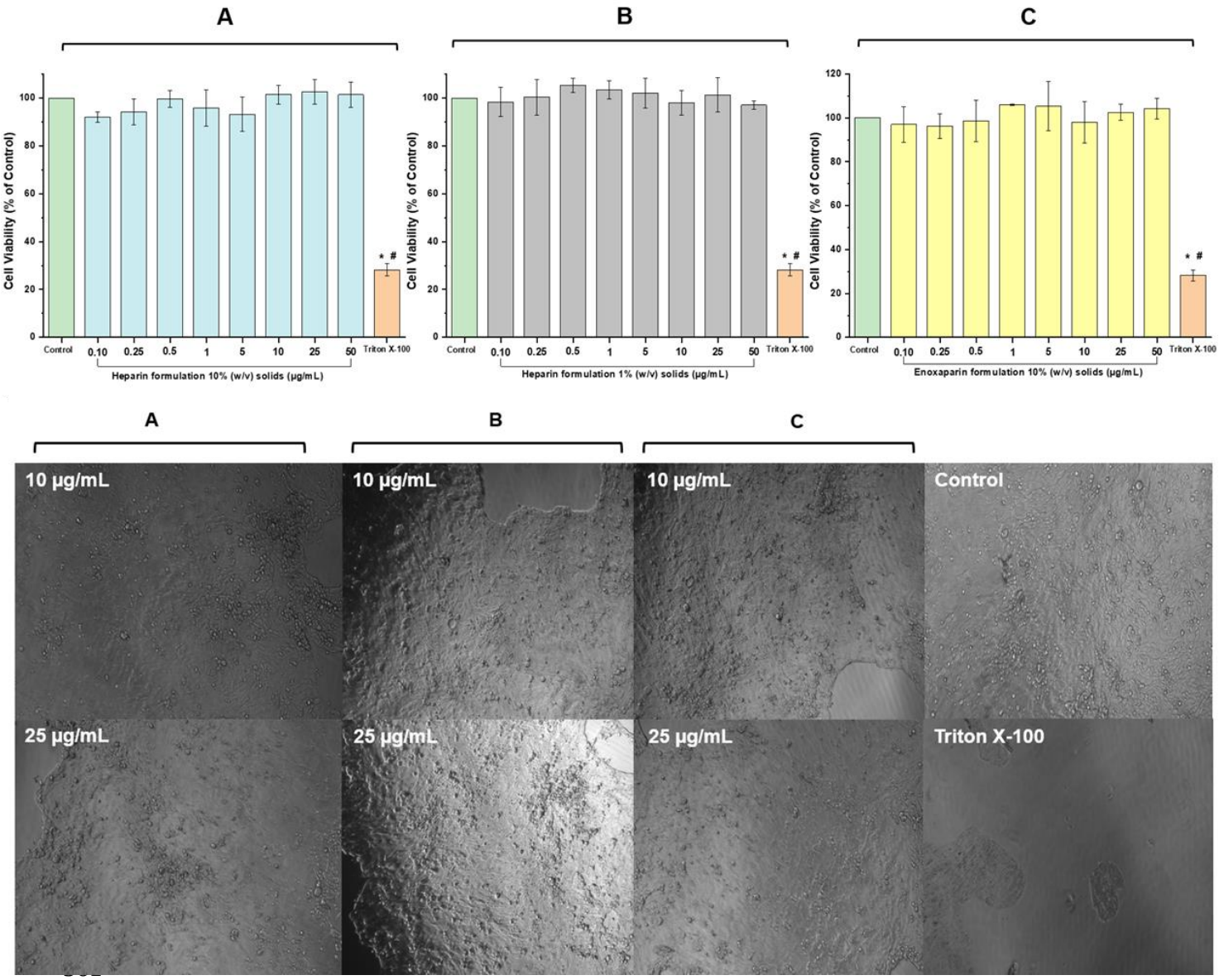

Figure 8. *in vitro* cytotoxicity MTT assay. Calu-3 cells were treated with **(A)** HF10%, **(B)** HF1%, and **(C)** EF10% at concentrations of AZM-loaded formulations from 0.1 µg/mL to 50.0 µg/mL for 24 h. Triton X-100 was used as a negative control. Data are expressed as mean ± SD (n = 9). *p < 0.05 vs control and #p < 0.05 *vs* formulations. Images were obtained with a Leica microscope at x10 magnification at 10 µg/mL and 25 µg/mL AZM concentration at 24 h.

Effect of AZM-loaded formulations on NO production in LPS-stimulated J774A.1 cells

Initially, the effect of AZM-loaded formulations on J774A.1 cell viability using MTT assay was examined. As shown in **Figure 9A-C**, no toxic effects were observed when cells were pretreated with any of the three AZM-loaded formulations (from 0.1 µg/mL to 50.0 µg/mL for 1 h) previous to LPS exposure (1 µg/mL for 24 h). As shown in **Figure 9-D1**, the three AZM-loaded formulations significantly suppressed the production of NO by LPS-stimulated J774A.1 cells in a concentration-dependent manner. **Figure 9-D2** shows the inhibition of NO

production at 10 µg/mL and 25 µg/mL concentrations. The selected concentrations were based on their relevance to the effective antibacterial range observed in previous assays against the targeted pathogens. This strategic selection allows for assessing the anti-inflammatory effects of the formulations at bactericidal concentrations offering an insight into their combined antibacterial and anti-inflammatory effects.

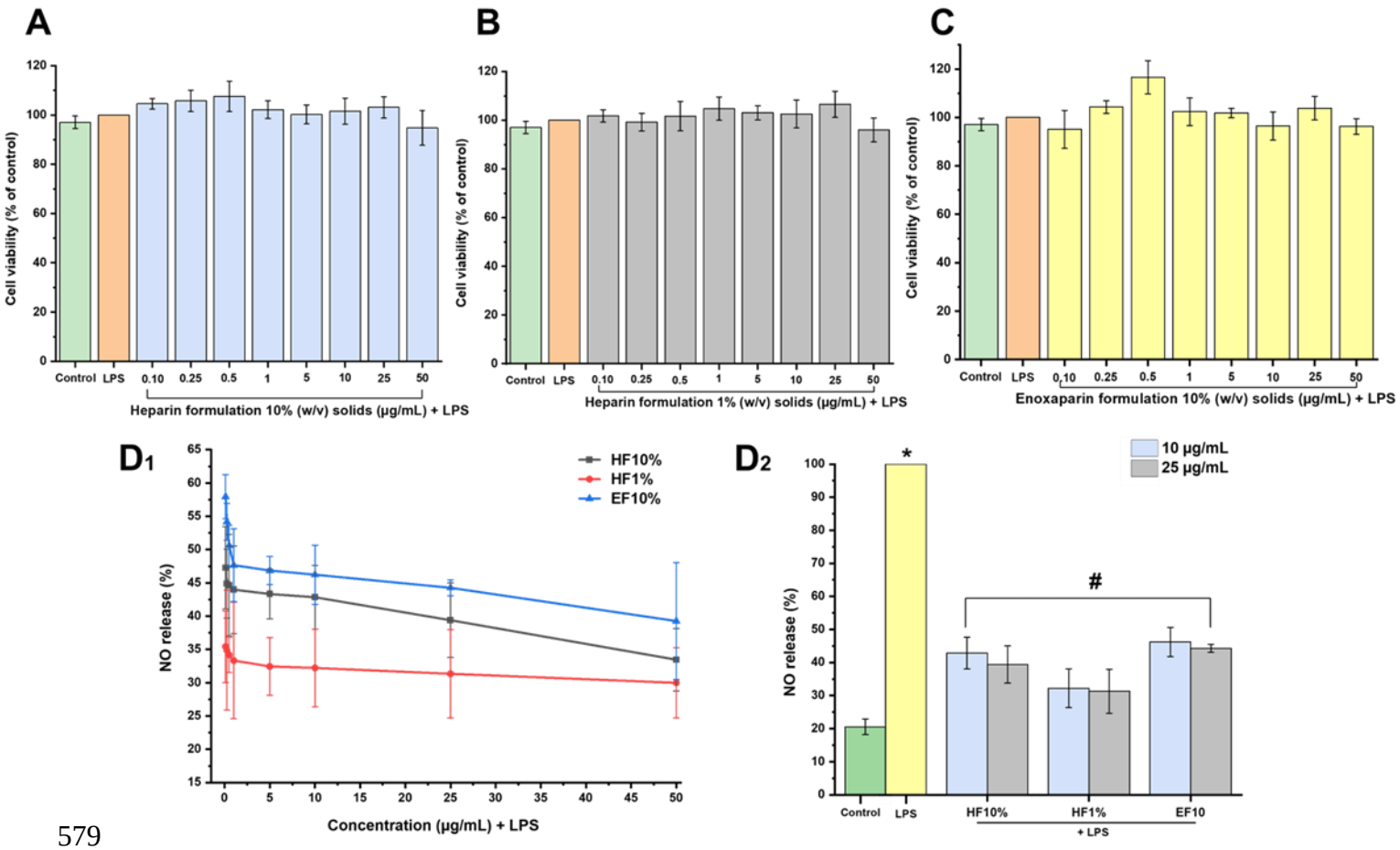

Figure 9. Effects of AZM-loaded formulations on J774A.1 cell viability and NO production. Cells were pre-treated with AZM-loaded formulations (from 0.1 µg/mL to 50.0 µg/mL for 1 h) following by LPS treatment (1 µg/mL for 24 h). Cell viability was determined using MTT assay (A) for HF10%, (B) for HF1% and (C) for EF10%. NO production was examined using Griess reagent assay (D1 and D2). Data are expressed as mean ± SD. *$p < 0.05$ vs control and #$p < 0.05$ *vs* LPS

4. Discussion

In this study, the antimicrobial efficacy of combined AZM and sulfated polysaccharides, namely heparin and its derivative enoxaparin, has been investigated for the first time. The negative charges of the polysaccharides can bind to positively charged bacterial surface molecules and host receptors, thereby regulating inflammatory responses to remove bacteria and reduce inflammation (Szekeres, et al. 2023; Voss, et al. 2013). Additionally, heparin and enoxaparin may enhance antibiotic penetration and biofilm destruction when combined with antibiotics, which could explain the reduction in the MIC concentration after

microencapsulation. In clinical practice, AZM has been investigated as a complementary treatment for chronic lung infections, including those caused by *P. aeruginosa* (Kumar, et al. 2021). AZM also reduces *P. aeruginosa* biofilm production, thereby improving the immune system sensitivity of the host. In the treatment, of multi-drug resistance (MDR) infections the combination of AZM with other antimicrobial drugs significantly reduced the total drug amount needed to combat bacteria (MIC_{50} and MIC_{90}) such as *P. aeruginosa* (Huang, et al. 2022; Tan, et al. 2016). Therefore, the observed enhanced efficacy between heparin and its derivatives and AZM within a DPI formulation can offer a focused and targeted therapeutic alternative for the treatment of lung infections.

Heparin and its derivatives exhibit significant pharmacological activities as anticoagulants and antithrombotic agents, crucial in addressing respiratory infections. In severe COVID-19, UFH and LMWH mitigate coagulopathy and thromboembolic complications (Iba, et al. 2020; Shute 2023). The primary anticoagulant function of heparin is mediated through its interaction with antithrombin, inhibiting key enzymes in the coagulation cascade. Notably, heparin's anti-inflammatory effects, including inhibition of chemokine activity and cytokine synthesis, are crucial in managing inflammatory lung diseases such as COVID-19, acute lung injury (ALI), and acute respiratory distress syndrome (ARDS) (Ashmawy, et al. 2023; Hogwood, et al. 2023; Shute, et al. 2018). Clinical applications have demonstrated heparin's potential to reduce mortality in COVID-19 patients by mitigating hypercoagulation and inflammation (Buijsers, et al. 2020; Qiu, et al. 2021a; Song, et al. 2024a; Walborn, et al. 2023).

Our AZM-loaded heparin microparticles showed similar MIC values against *S. aureus*, but were 10 times more effective against *P. aeruginosa*, which are among the most common causative agents of respiratory infections (Arauzo, et al. 2021b). One major advantage of the AZM-loaded heparin microparticles was their high biocompatibility on Calu-3 and RBCs, indicating a large therapeutic window for clinical use.

Nitric oxide (NO) is a pro-inflammatory mediator in LPS-stimulated J774A.1 cells, playing a crucial role in the inflammatory response (Bogdan 2015). In our study, NO production by LPS-stimulated J774A.1 cells was significantly reduced by the AZM-loaded formulations. These results are consistent with previous studies that demonstrate the anti-inflammatory effects of AZM in macrophages (Banjanac, et al. 2012; Zimmermann, et al. 2018) and also aligns with the available evidence for the efficacy and safety of inhaled heparin in improving lung functions among asthmatic and COPD patients (Ashmawy 2023). Additionally, the formulations at concentrations of 10 μg/mL and 25 μg/mL exhibited anti-inflammatory. These concentrations, achievable in lung tissue after inhaled administration of AZM, underscore the clinical relevance of our findings (Davidson 2019).

The aerodynamic deposition pattern has demonstrated effective alveolar deposition, with appropriate MMAD (1 μm - 3 μm). Depending on the percentage of solids in the formulation

before spray drying, the MMAD can be tuned and adjusted to meet the clinical needs. For infections occurring in the upper respiratory tract, a higher deposition in the first stages is required, which can be achieved with a higher content of solids (10 %). Conversely, for deeper lung infections, targeting drug deposition towards the latter stages of the NGI is recommended. This can be achieved by reducing the percentage of solid material in the suspension prepared before spray drying (from 10 % to 1 %). This ability to target lung deposition is crucial to ensure a broad spectrum against bacteria and viruses located in different regions of the respiratory tract.

Currently, nebulized solutions heparin and enoxaparin for acute respiratory distress and coagulopathy associated with COVID-19 are a focal point of research. However, DPIs offer several advantages over the nebulized therapies, including enhanced patient compliance and the ability to deliver larger doses of heparin/enoxaparin directly to the lungs (Ceccato, et al. 2022; Eder, et al. 2022; Erelel, et al. 2021; Van Haren, et al. 2020). Bai et al. (2010) (Bai, et al. 2010) evaluated different DPI formulations of LMWH by mixing it with lactose to improve lung delivery. This resulted in a much higher particle size (11.6 μm ± 5.8 μm and 16.7 μm ± 5.5 μm) and hence, poorer lung deposition compared to our AZM-loaded heparin microparticles.

A prospective observational study demonstrated that nebulized UFH improves oxygenation and reduces lung damage in COVID-19 patients with ARDS, using 5,000 units/mL of heparin diluted in 3 mL of 0.9 % sodium chloride every 6 h for 7 days (Gupta, et al. 2023). In our study, each capsule was filled with 25 mg of powder, equivalent to 20 mg of heparin or enoxaparin and about 1 mg of AZM. In each administration, considering the FPF deposited in the lung (< 5 μm), approximately 10 mg (1,000 units) of heparin and enoxaparin and 0.5 mg of AZM can be delivered in each administration. Adopting a conservative estimate of 20 mL for the pulmonary epithelial lining fluid (Trenfield, et al.) volume in healthy adults, as reported in the literature with a typical range of 10 - 30 mL (Altay Benetti, et al. 2021). The calculated concentration of heparin or enoxaparin in the ELF would approximate 500 μg/mL and for AZM, 25 μg/mL. However, it is imperative to acknowledge that this value may be subject to variation contingent upon individual differences in ELF volume, mucociliary clearance mechanisms, absorption kinetics, and metabolic processes governing the fate of these compounds. This delivery is expected to contribute to restoring lung function treating and preventing from microbial growth.

Conzelmann *et al.* (2020) (Conzelmann, et al. 2020) demonstrated that heparin inhibits SARS-CoV-2 *in vitro* infection in Vero E6 cells. Higher concentrations of heparin not only reduced the overall number of plaques but also drastically diminished their size, indicating potent suppression (60 %) of viral spread and replication at the concentration above 125 μg/mL. In our DPI formulation, heparin showed a more potent effect in inhibiting virus propagation compared to enoxaparin. This difference may be attributed to heparin's larger molecular weight and its ability to bind the virus more effectively. It appears counterintuitive,

given the general principle that compounds with reduced molecular weight tend to exhibit greater potency. However, it implies that the broader molecular weight distribution of unfractionated heparin may provide specific structural advantages, aiding anchoring to receptor, providing less flexibility or binding interactions that enable more potent inhibition of viral propagation at lower concentrations compared to the more uniform, but lower molecular weight, enoxaparin. Alternative mechanisms of action that target distinct phases in the viral life cycle, increased cell permeability of specific heparin fractions, or favorable binding to critical viral or host cell targets are potential factors that could also contribute to this enhanced potency.

In another study by Tandon *et al.* (2021) (Tandon, et al. 2021), a lentiviral vector was pseudotyped with the SARS-CoV-2 spike glycoprotein to facilitate viral attachment and entry. Sulfated polysaccharides, including UFH and enoxaparin, were evaluated for pseudotyped viral neutralization, demonstrating strong anti-SARS-CoV-2 activity by preventing viral entry at low concentrations (IC_{50} values: 0.00599 μg/mL for UFH and 1.08 μg/mL for enoxaparin). In our study, AZM-loaded microparticle formulations exhibit remarkably potent antiviral activity against SARS-CoV-2, with IC_{50} values in the low nanomolar range (13.5 nM and 95.0 nM for HF10% and EF10% respectively). The high antibacterial efficacy, combined with a strong anti-SARS-CoV-2 activity, makes the AZM-loaded microparticulate formulations promising candidates for the treatment and prevention of COVID-19 associated with bacterial infections.

Alternative excipients such as calcium carbonate, maltose, mannitol, and lactose can enhance DPI formulation stability and aerosolization. However, leucine's versatility across various drug types and its established safety profile for inhalation render it superior for optimizing lung deposition in DPI formulations (Altay Benetti, et al. 2021; Shalash and Elsayed 2017; Sharif, et al. 2023; Walther, et al. 2022; Wang, et al. 2023a). As previously demonstrated, the incorporation of leucine in the AZM-loaded microparticles significantly improves the flow properties of DPIs, making them to reach deeper regions of the respiratory tract (Celi, et al. 2023a; Xu, et al. 2022). Leucine also can augment drug dissolution without compromising aerosol performance. This enhancement is achieved through the formation of a composite system with AZM and the creation of an acidic microenvironment during dissolution. These mechanisms synergistically increase AZM solubility, potentially amplifying its antimicrobial efficacy (Mangal, et al. 2018; Mangal, et al. 2019).

Similar results were observed when leucine was incorporated into sulfated polysaccharides microparticles. The concomitant administration of AZM presents therapeutic advantages in the clinical management of chronic respiratory conditions, including post-lung transplantation sequelae, idiopathic pulmonary fibrosis, cystic fibrosis therapy, and reduction in inflammatory processes within the respiratory tract (Morlacchi, et al. 2022; Shur, et al. 2008b; Wuyts, et al. 2010). The overall optimal deposition profile, along with the demonstrated *in vitro* safety and efficacy, presents a novel approach to combat COVID-19

progression with bacterial infections. However, further pharmacokinetic studies are needed to confirm the *in vitro* deposition profile and evaluate the systemic effects of the formulations.

Conclusion

The development of DPI formulations combining AZM with sulfated polysaccharides, such as UFH and derivatives, offers a promising multifaceted approach for treating bacterial lung infections associated with COVID-19. This strategy leverages the antimicrobial and anti-inflammatory properties of AZM, which accumulates in lung tissues after administration, together with the antiviral potential of sulfated polysaccharides to block SARS-CoV-2 propagation. The microparticle formulations exhibited potent antiviral activity while maintaining antibacterial efficacy against common respiratory pathogens, comparable or even superior to unprocessed AZM. Furthermore, AZM-loaded microparticulate formulations demonstrated a favorable safety profile even at high concentrations (50 µg/mL), with optimised deposition profile within the respiratory tract. However, further *in vivo* studies need to be performed to confirm the pharmacological-toxicological profile.

Acknowledgments

Thanks to Eva Batanero Cremades from the Department of Biochemistry and Molecular Biology, Faculty of Chemistry, Complutense University of Madrid, Madrid, Spain, for donating Calu-3 cells. Brayan J. Anaya thanks the Ministerio de Ciencia Tecnología e Innovación (MinCiencias) of Colombia, Call No. 885 of 2020, for the doctoral scholarship. This study has also been partially funded by the Spanish Ministry of Science and Innovation (award PID2021-126310OA-I00 to Dolores Serrano) and the Universidad Nacional de Colombia (project reference 58990).

References

COVID-19 Coronavirus Receptor Stable Cell Lines. Available at: https://www.genecopoeia.com/product/covid-19-coronavirus-stable-cell-lines/. Accessed date: 8 June 2024.

Ahmad, F. B., et al.

2023 COVID-19 Mortality Update - United States, 2022. MMWR Morb Mortal Wkly Rep 72(18):493-496.

Al-Hakkani, Mostafa F

2019 A rapid, developed and validated RP-HPLC method for determination of azithromycin. SN Applied Sciences 1(3):222.

Albert, Richard K, et al.

2011 Azithromycin for prevention of exacerbations of COPD. New England Journal of Medicine 365(8):689-698.

Alipour, Shohreh, Laleh Mahmoudi, and Fatemeh Ahmadi

2023 Pulmonary drug delivery: an effective and convenient delivery route to combat COVID-19. Drug delivery and translational research 13(3):705-715.

748 Altay Benetti, Ayça, et al.

749 2021 Mannitol polymorphs as carrier in DPIs formulations: isolation
750 characterization and performance. Pharmaceutics 13(8):1113.
751 Annisa, Rahmi, et al.

752 2023 NANOTECHNOLOGY APPROACH-SELF NANOEMULSIFYING DRUG
753 DELIVERY SYSTEM (SNEDDS). International Journal of Applied Pharmaceutics
754 15(4):12-19.
755 Arauzo, Beatriz, et al.

756 2021a Dry powder formulation for pulmonary infections: Ciprofloxacin loaded in
757 chitosan sub-micron particles generated by electrospray. Carbohydrate Polymers
758 273:118543.
759 Arauzo, Beatriz, et al.

760 2021b Excipient-free inhalable microparticles of azithromycin produced by
761 electrospray: a novel approach to direct pulmonary delivery of antibiotics.
762 Pharmaceutics 13(12):1988.
763 Ashmawy, Rasha, et al.

764 2023 Efficacy and safety of inhaled heparin in asthmatic and chronic obstructive
765 pulmonary disease patients: a systematic review and a meta-analysis. Scientific
766 Reports 13(1):13326.
767 Bai, Shuhua, Vivek Gupta, and Fakhrul Ahsan

768 2010 Inhalable lactose-based dry powder formulations of low molecular weight
769 heparin. Journal of aerosol medicine and pulmonary drug delivery 23(2):97-104.
770 Bai, Xiyuan, et al.

771 2022 Enoxaparin augments alpha-1-antitrypsin inhibition of TMPRSS2, a
772 promising drug combination against COVID-19. Scientific reports 12(1):5207.
773 Ballacchino, G., et al.

774 2021 Manufacturing of 3D-Printed Microfluidic Devices for the Synthesis of
775 Drug-Loaded Liposomal Formulations. Int J Mol Sci 22(15).
776 Banjanac, Mihailo, et al.

777 2012 Anti-inflammatory mechanism of action of azithromycin in LPS-stimulated
778 J774A. 1 cells. Pharmacological research 66(4):357-362.
779 Belanger, Corrie R, et al.

780 2020 Identification of novel targets of azithromycin activity against Pseudomonas
781 aeruginosa grown in physiologically relevant media. Proceedings of the National
782 Academy of Sciences 117(52):33519-33529.
783 Bogdan, Christian

784 2015 Nitric oxide synthase in innate and adaptive immunity: an update. Trends in
785 immunology 36(3):161-178.
786 Buijsers, Baranca, et al.

2020 Beneficial non-anticoagulant mechanisms underlying heparin treatment of COVID-19 patients. EBioMedicine 59.
Calabrò, Luana, et al.

2021 COVID and lung cancer. Current oncology reports 23:1-10.
Ceccato, Adrian, et al.

2022 Anticoagulant treatment in severe ARDS COVID-19 patients. Journal of clinical medicine 11(10):2695.
Celi, S. S., et al.

2023a Co-Delivery of a High Dose of Amphotericin B and Itraconazole by Means of a Dry Powder Inhaler Formulation for the Treatment of Severe Fungal Pulmonary Infections. Pharmaceutics 15(11).
Celi, Salomé S, et al.

2023b Co-Delivery of a High Dose of Amphotericin B and Itraconazole by Means of a Dry Powder Inhaler Formulation for the Treatment of Severe Fungal Pulmonary Infections. Pharmaceutics 15(11):2601.
Cerier, Emily, et al.

2023 Lung transplantation in coronavirus-19 patients: What we have learned so far. Clinics in Chest Medicine 44(2):347-357.
Clausen, Thomas Mandel, et al.

2020 SARS-CoV-2 infection depends on cellular heparan sulfate and ACE2. Cell 183(4):1043-1057. e15.
Conzelmann, Carina, et al.

2020 Inhaled and systemic heparin as a repurposed direct antiviral drug for prevention and treatment of COVID-19. Clinical Medicine 20(6):e218.
D'Angelo, Davide, et al.

2023 An Enhanced Dissolving Cyclosporin-A Inhalable Powder Efficiently Reduces SARS-CoV-2 Infection In Vitro. Pharmaceutics 15(3):1023.
Davidson, Ross J

2019 In vitro activity and pharmacodynamic/pharmacokinetic parameters of clarithromycin and azithromycin: why they matter in the treatment of respiratory tract infections. Infection and drug resistance:585-596.
de Boer, Anne H, et al.

2017 Dry powder inhalation: past, present and future. Expert opinion on drug delivery 14(4):499-512.
de Pablo, E, et al.

2023 Targeting lung macrophages for fungal and parasitic pulmonary infections with innovative amphotericin B dry powder inhalers. International Journal of Pharmaceutics 635:122788.
de Pablo, Esther, et al.

2017 Nebulised antibiotherapy: conventional versus nanotechnology-based approaches, is targeting at a nano scale a difficult subject? Annals of translational medicine 5(22).
DeBiase, Christopher, et al.

2021 Enoxaparin versus unfractionated heparin for venous thromboembolism prophylaxis in renally impaired ICU patients. Pharmacotherapy: The Journal of Human Pharmacology and Drug Therapy 41(5):424-429.
Eder, Julia, et al.

2022 Inhalation of Low Molecular Weight Heparins as Prophylaxis against SARS-CoV-2. Mbio 13(6):e02558-22.
Eilts, Friederike, et al.

2023 The diverse role of heparan sulfate and other GAGs in SARS-CoV-2 infections and therapeutics. Carbohydrate Polymers 299:120167.
Erelel, M, et al.

2021 Early Effects of Low Molecular Weight Heparin Therapy with Soft-Mist Inhaler for COVID-19-Induced Hypoxemia: A Phase IIb Trial. Pharmaceutics 2021, 13, 1768: s Note: MDPI stays neu-tral with regard to jurisdictional claims in ….
Feng, Ke, et al.

2023 Non-Anticoagulant Activities of Low Molecular Weight Heparins—A Review. Pharmaceuticals 16(9):1254.
Ferrand, R, et al.

2020 Effect of Once-Weekly Azithromycin vs Placebo in Children With HIV-Associated Chronic Lung Disease: The BREATHE Randomized Clinical Trial. JAMA Netw open2020; 3. DOI: https://doi. org/10.1001/jamanetworkopen.
Franco-Palacios, Domingo, et al.

2023 Lung Transplantation for COVID-19 Related Lung Disease: A Follow-Up Study of Outcomes from a Medium-Size Lung Transplant Programd. OBM Transplantation 7(3):1-25.
Galrinho, Miguel F, et al.

2024 The study of galactomannans with different molecular weights and their ability to form microparticles suitable for pulmonary delivery. Carbohydrate Polymers 339:122268.
Gingras, Hélène, et al.

2020 Azithromycin resistance mutations in Streptococcus pneumoniae as revealed by a chemogenomic screen. Microbial Genomics 6(11):e000454.
guidelines, Clinical Laboratory Standards Institute (CLSI)

minimum inhibitory concentration (MIC) Vol. 2024.
Güler, Hülya Kesici, and Funda Cengiz Çallioğlu

2023 Suspension electrospinning of azithromycin loaded nanofibers. Journal of Drug Delivery Science and Technology 88:104947.

Gupta, Bhavna, et al.

2023 Nebulized heparin to reduce COVID-19-induced acute lung injury: a prospective observational study. Indian Journal of Critical Care Medicine: Peer-reviewed, Official Publication of Indian Society of Critical Care Medicine 27(3):222.

Hogwood, John, et al.

2023 Pharmacology of heparin and related drugs: An update. Pharmacological reviews 75(2):328-379.

Huang, Yuqin, et al.

2022 Clinical efficacy and in vitro drug sensitivity test results of azithromycin combined with other antimicrobial therapies in the treatment of mdr p. Aeruginosa ventilator-associated pneumonia. Frontiers in Pharmacology 13:944965.

Iba, Toshiaki, et al.

2020 Coagulopathy of coronavirus disease 2019. Critical care medicine 48(9):1358-1364.

Jabeen, Mehwish, et al.

2021 Seaweed sulfated polysaccharides against respiratory viral infections. Pharmaceutics 13(5):733.

Jones, Ronald N, et al.

1994 Validation of NCCLS macrolide (azithromycin, clarithromycin, and erythromycin) interpretive criteria for Haemophilus influenzae tested with the Haemophilus test medium. Diagnostic microbiology and infectious disease 18(4):243-249.

Kilic, Hatice, et al.

2022 Effect of chronic lung diseases on mortality of prevariant COVID-19 pneumonia patients. Frontiers in Medicine 9:957598.

Kumar, Manoj, et al.

2021 Azithromycin exhibits activity against Pseudomonas aeruginosa in chronic rat lung infection model. Frontiers in Microbiology 12:603151.

Leal, Teresinha, et al.

2016 Azithromycin attenuates Pseudomonas-induced lung inflammation by targeting bacterial proteins secreted in the cultured medium. Frontiers in immunology 7:499.

Lu, Wenjing, et al.

2021 Recent advances in antiviral activities and potential mechanisms of sulfated polysaccharides. Carbohydrate Polymers 272:118526.

Mangal, Sharad, et al.

2018 Physico-chemical properties, aerosolization and dissolution of co-spray dried azithromycin particles with l-leucine for inhalation. Pharmaceutical research 35:1-15.

Mangal, Sharad, et al.

2019 Understanding the impacts of surface compositions on the in-vitro dissolution and aerosolization of co-spray-dried composite powder formulations for inhalation. Pharmaceutical research 36:1-15.

Molina, Carlos, et al.

2018 Agglomerated novel spray-dried lactose-leucine tailored as a carrier to enhance the aerosolization performance of salbutamol sulfate from DPI formulations. Drug delivery and translational research 8:1769-1780.

Morlacchi, L, et al.

2022 Effects of Azithromycin in Lung Transplant Recipients. The Journal of Heart and Lung Transplantation 41(4):S290-S291.

Oliver, Madeleine E, and Timothy SC Hinks

2021 Azithromycin in viral infections. Reviews in medical virology 31(2):e2163.

Özbek, Laşin, et al.

2023 COVID-19-associated mucormycosis: a systematic review and meta-analysis of 958 cases. Clinical Microbiology and Infection.

Pineros, Isabel, et al.

2017 Analgesic and anti-inflammatory controlled-released injectable microemulsion: Pseudo-ternary phase diagrams, in vitro, ex vivo and in vivo evaluation. European journal of pharmaceutical sciences 101:220-227.

Pradhan, Biswajita, et al.

2022 A state-of-the-art review on fucoidan as an antiviral agent to combat viral infections. Carbohydrate Polymers 291:119551.

Qiu, Min, et al.

2021a Pharmacological and clinical application of heparin progress: An essential drug for modern medicine. Biomedicine & Pharmacotherapy 139:111561.

Qiu, Xiao-Lei, et al.

2021b Preparation and evaluation of a self-nanoemulsifying drug delivery system loaded with heparin phospholipid complex. International Journal of Molecular Sciences 22(8):4077.

Ramaiah, Balakeshwa, et al.

2016 High azithromycin concentration in lungs by way of bovine serum albumin microspheres as targeted drug delivery: lung targeting efficiency in albino mice. DARU Journal of Pharmaceutical Sciences 24:1-11.

Rehfeld, Anders, Malin Nylander, and Kirstine Karnov

2017 The Respiratory System. *In* Compendium of Histology: A Theoretical and Practical Guide. Pp. 351-377. Cham: Springer International Publishing.

Ruiz, Helga K, et al.

2022 Current Treatments for COVID-19: Application of Supercritical Fluids in the Manufacturing of Oral and Pulmonary Formulations. Pharmaceutics 14(11):2380.

946 Shalash, Ahmed O, and Mustafa MA Elsayed

947 2017 A new role of fine excipient materials in carrier-based dry powder inhalation
948 mixtures: effect on deagglomeration of drug particles during mixing revealed.
949 AAPS PharmSciTech 18(8):2862-2870.
950 Sharif, Shahjabeen, et al.

951 2023 Impact of leucine and magnesium stearate on the physicochemical properties
952 and aerosolization behavior of wet milled inhalable ibuprofen microparticles for
953 developing dry powder inhaler formulation. Pharmaceutics 15(2):674.
954 Shi, Chen, et al.

955 2021 Comprehensive landscape of heparin therapy for COVID-19. Carbohydrate
956 polymers 254:117232.
957 Shi, Fang-Shu, et al.

958 2024 Fucoidan from Ascophyllum nodosum and Undaria pinnatifida attenuate
959 SARS-CoV-2 infection in vitro and in vivo by suppressing ACE2 and alleviating
960 inflammation. Carbohydrate Polymers 332:121884.
961 Shur, J., et al.

962 2008a The spray drying of unfractionated heparin: optimization of the operating
963 parameters. Drug Dev Ind Pharm 34(6):559-68.
964 Shur, Jagdeep, et al.

965 2008b Cospray-dried unfractionated heparin with L-leucine as a dry powder inhaler
966 mucolytic for cystic fibrosis therapy. Journal of pharmaceutical sciences
967 97(11):4857-4868.
968 Shute, Janis K, Ermanno Puxeddu, and Luigino Calzetta

969 2018 Therapeutic use of heparin and derivatives beyond anticoagulation in
970 patients with bronchial asthma or COPD. Current Opinion in Pharmacology 40:39-
971 45.
972 Shute, Janis Kay

973 2023 Heparin, low molecular weight heparin, and non-anticoagulant derivatives
974 for the treatment of inflammatory lung disease. Pharmaceuticals 16(4):584.
975 Smith, Lindsay, et al.

976 2018 Orally bioavailable and effective buparvaquone lipid-based nanomedicines
977 for visceral leishmaniasis. Molecular pharmaceutics 15(7):2570-2583.
978 Song, Ying, et al.

979 2024a The Preventive and Therapeutic Effects of Acute and Severe Inflammatory
980 Disorders with Heparin and Heparinoid. Biomolecules 14(9):1078.
981 Song, Yuefan, et al.

982 2024b Seaweed-derived fucoidans and rhamnan sulfates serve as potent anti-SARS-
983 CoV-2 agents with potential for prophylaxis. Carbohydrate Polymers 337:122156.
984 Szekeres, Gergo Peter, et al.

2023 Heparin increases the antibiotic efficacy of colistin. Frontiers in Analytical Science 3:1154391.

Tan, Hao, et al.

2016 PA3297 counteracts antimicrobial effects of azithromycin in Pseudomonas aeruginosa. Frontiers in microbiology 7:182864.

Tan, Rebecca Shu Ling, et al.

2022 Chitosan and its derivatives as polymeric anti-viral therapeutics and potential anti-SARS-CoV-2 nanomedicine. Carbohydrate Polymers 290:119500.

Tandon, Ritesh, et al.

2021 Effective inhibition of SARS-CoV-2 entry by heparin and enoxaparin derivatives. Journal of Virology 95(3):10.1128/jvi. 01987-20.

Trenfield, Sarah J, et al.

2018 3D printed drug products: Non-destructive dose verification using a rapid point-and-shoot approach. International journal of pharmaceutics 549(1-2):283-292.

Troeger, Christopher, et al.

2018 Estimates of the global, regional, and national morbidity, mortality, and aetiologies of lower respiratory infections in 195 countries, 1990–2016: a systematic analysis for the Global Burden of Disease Study 2016. The Lancet infectious diseases 18(11):1191-1210.

Van Haren, Frank MP, et al.

2020 Nebulised heparin as a treatment for COVID-19: scientific rationale and a call for randomised evidence. Critical Care 24:1-11.

Veeranki, S Phani, et al.

2021 Real-world comparative effectiveness and cost comparison of thromboprophylactic use of enoxaparin versus unfractionated heparin in 376,858 medically ill hospitalized US patients. American Journal of Cardiovascular Drugs 21:443-452.

Vehring, Reinhard

2008 Pharmaceutical particle engineering via spray drying. Pharmaceutical research 25(5):999-1022.

Voss, Sylvia, et al.

2013 The choline-binding protein PspC of Streptococcus pneumoniae interacts with the C-terminal heparin-binding domain of vitronectin. Journal of Biological Chemistry 288(22):15614-15627.

Walborn, Amanda T, et al.

2023 Effects of inflammation on thrombosis and outcomes in COVID-19: secondary analysis of the ATTACC/ACTIV-4a trial. Research and Practice in Thrombosis and Haemostasis 7(7):102203.

Walther, Frans J, et al.

2022 Efficacy, dose–response, and aerosol delivery of dry powder synthetic lung surfactant treatment in surfactant-deficient rabbits and premature lambs. Respiratory Research 23(1):78.

Wang, Bo, et al.

2023a Enhancing bioavailability of natural extracts for nutritional applications through dry powder inhalers (DPI) spray drying: technological advancements and future directions. Frontiers in Nutrition 10:1190912.

Wang, Lu, et al.

2023b ROS-sensitive Crocin-loaded chitosan microspheres for lung targeting and attenuation of radiation-induced lung injury. Carbohydrate Polymers 307:120628.

Wang, Peipei, et al.

2022 Heparin: An old drug for new clinical applications. Carbohydrate Polymers 295:119818.

Watson, Ol, et al.

2023 The efficacy of low molecular weight heparin is reduced in COVID-19. Clinical Hemorheology and Microcirculation 84(3):333-344.

Wong, Chun Yuen Jerry, et al.

2022 Validation of a cell integrated next-generation impactor to assess in vitro drug transport of physiologically relevant aerosolised particles. International Journal of Pharmaceutics 624:122024.

Wuyts, WA, et al.

2010 Azithromycin reduces pulmonary fibrosis in a bleomycin mouse model. Experimental lung research 36(10):602-614.

Xiang, Yufei, et al.

2020 Versatile and multivalent nanobodies efficiently neutralize SARS-CoV-2. Science 370(6523):1479-1484.

Xu, You, et al.

2022 Inhalable composite microparticles containing siRNA-loaded lipid-polymer hybrid nanoparticles: Saccharides and leucine preserve aerosol performance and long-term physical stability. Frontiers in Drug Delivery 2:945459.

Zhu, Na, et al.

2020 A novel coronavirus from patients with pneumonia in China, 2019. New England journal of medicine 382(8):727-733.

Zimmermann, Petra, et al.

2018 The immunomodulatory effects of macrolides—a systematic review of the underlying mechanisms. Frontiers in immunology 9:302.